# A Two-Stage Stochastic Optimization Model for Scheduling Electric Vehicle Charging Loads to Relieve Distribution-System Constraints

Fei Wu, Ramteen Sioshansi*

*Integrated Systems Engineering Department, The Ohio State University, Columbus, Ohio, United States of America*
*Phone: +1-614-292-3932*

**Abstract**

Electric vehicles (EVs) hold promise to improve the energy efficiency and environmental impacts of transportation. However, widespread EV use can impose significant stress on electricity-distribution systems due to their added charging loads.

This paper proposes a centralized EV charging-control model, which schedules the charging of EVs that have flexibility. This flexibility stems from EVs that are parked at the charging station for a longer duration of time than is needed to fully recharge the battery. The model is formulated as a two-stage stochastic optimization problem. The model captures the use of distributed energy resources and uncertainties around EV arrival times and charging demands upon arrival, non-EV loads on the distribution system, energy prices, and availability of energy from the distributed energy resources. We use a Monte Carlo-based sample-average approximation technique and an L-shaped method to solve the resulting optimization problem efficiently. We also apply a sequential sampling technique to dynamically determine the optimal size of the randomly sampled scenario tree to give a solution with a desired quality at minimal computational cost.

We demonstrate the use of our model on a Central-Ohio-based case study. We show the benefits of the model in reducing charging costs, negative impacts on the distribution system, and unserved EV-charging demand compared to simpler heuristics. We also conduct sensitivity analyses, to show how the model performs and the resulting costs and load profiles when the design of the station or EV-usage parameters are changed.

*Keywords:* Electric vehicle, vehicle charging, charging control, stochastic optimization, sample-average approximation

## 1. Introduction

Electric vehicles (EVs) hold great promise to improve the energy efficiency and environmental impacts of transportation. However, widespread EV use brings uncertain impacts to electric power systems, especially at the distribution level. Clement-Nyns et al. (2010) find that uncontrolled EV charging (*i.e.*, EVs charging without any coordination) can result in power losses and voltage deviations on the local distribution network. Razeghi et al. (2014) study the impacts of charging 10 EVs in an uncontrolled fashion on a residential transformer. They demonstrate that the resulting charging loads can result in catastrophic failure of the transformer and conclude that management of charging loads is critical for prolonging transformer life. Weiller (2011) estimates the impacts of EV recharging using standard wall outlets on electric loads in the United States. The results of this analysis show that residential, workplace, and retail-shopping-center loads can be increased by 74%.

*Corresponding author
*Email addresses:* wu.1557@osu.edu (Fei Wu), sioshansi.1@osu.edu (Ramteen Sioshansi)

One way to accommodate these impacts of widespread EV use is to upgrade distribution-system infrastructure, including transformers. This solution would see the distribution system sized to accommodate the anticipated peak load. Indeed, because distribution-infrastructure investments are typically long-lived (*e.g.*, most distribution transformers have a design life of 20.5 years), the system would be sized based on anticipated future peak loads. This is an inefficient solution, however, because the peak load on many distribution circuits may only be reached a few hours each year. This means that the distribution system would have excess unused capacity the overwhelming majority of the time. Uncontrolled EV charging may exacerbate this inefficiency, because uncontrolled EV charging tends to give the distribution load profile more extreme peaks.

An alternate solution is control or management of EV-charging loads. The basic premise of charging control is that an EV may be connected to a charging station for a longer duration of time than is required to fully recharge its battery. If so, the charging demand could be shifted within this window of time. By properly managing such flexible EV loads, the peaks in the distribution load profile can be reduced, alleviating the need for expensive transformer upgrades. Moreover, controlling EV charging can increase the load factor of the distribution system, meaning that the distribution infrastructure is used more efficiently.

The literature typically focuses on two forms of EV-charging control: centralized and decentralized. Decentralized control is a price-signal based method to coordinate EV charging. This method usually requires individual EVs and an EV aggregator to communicate their demands for charging energy and the availability of energy in an iterative before reaching an equilibrium. In this context, an equilibrium is a set of charging loads that are optimal from the perspective of the EVs (*i.e.*, it satisfies their demands for charging energy) and the EV aggregator (*i.e.*, the aggregator can feasibly serve the charging loads). Ma et al. (2013) introduce a price-based decentralized control scheme. In their proposal, EVs communicate their charging demands iteratively based on a set pricing scheme. They demonstrate that the iterative scheme can reach an equilibrium under mild conditions. Wu et al. (2012) propose a decentralized scheme which uses a price policy that encourages individual EVs to provide frequency regulation. Bayram et al. (2013) propose an admission-control mechanism that applies congestion pricing to mitigate station-level overloads and guarantee quality of service among EVs. Xi and Sioshansi (2014) introduce a decentralized pricing scheme that conveys both price and quantity from the power system operator to an EV aggregator or to individual EVs.

Conversely, centralized control relies on a single entity to manage EV charging. Thus, it relies on EV owners letting someone else determine when their vehicles are recharged. Sathaye (2014) proposes an optimization framework for an electrified taxi-service operator to schedule taxi-charging loads. This approach takes the optimality and feasibility of the transportation system into account, assuming a Level-2 DC charging station and that the power system can always fulfill the station's charging demand. This approach taken by Sathaye (2014) differs from many other works examining charging management. Sathaye (2014) assumes that the power system can always serve charging loads and optimizes charging from the perspective of the taxi service. Many other works, conversely, focus on optimality and feasibility, taking into account that the power system may not be able to accommodate charging loads that are not properly managed. For instance, Hu et al. (2014) introduce a linear programming model that determines an optimal EV-charging schedule to minimize charging cost to an EV aggregator while preventing distribution-system congestion. Rotering and Ilić (2011) propose a dynamic programming model to control and optimize accumulated EV-charging demand. Sundström and Binding (2012) develop a quadratic programming model that minimizes the operation cost of an EV aggregator's operation cost while imposing distribution-network constraints.

More recent works pay increasing attention to uncertainty in when EVs may arrive at a charging station and their charging demands upon arrival. Pantoš (2012) proposes a stochastic optimization model with uncertainty in EV-usage patterns to create strategies for an individual EV that wants to participate in energy and ancillary service markets by providing charging flexibility. Momber et al. (2015) introduce an EV-charging control model for a risk-averse EV aggregator. They use conditional value-at-risk as the risk metric in the objective function. Their work focuses on modeling uncertainty in EV-usage patterns and energy prices.

The use of stochastic optimization techniques typically raises computational challenges, because of the immense number of scenarios needed to capture all of the uncertainties modeled. Pantoš (2012); Momber et al. (2015) deal with this issue through scenario reduction, wherein a large starting set of scenarios is reduced to

a smaller set that is meant to represent the range of possible sample paths in the starting set of scenarios. This use of scenario reduction raises two important and related questions, however. The first is whether scenario reduction guarantees a high-quality solution. The second is how to choose appropriate starting and reduced sample sizes that give a desired solution quality with the least amount of computational effort. This second issue is especially important if a charging-control model is to be used for actual real-time control of EV-charging loads.

In this paper we introduce a centralized control model that concentrates on high-power fast-charging stations. The aim of the model is to optimize EV-charging loads within a fixed window of time after each EV arrives at the charging station to minimize costs. The costs modeled include a penalty, based on the associated accelerated aging, of operating the distribution transformer above its rated capacity. The core methodology of our approach is a two-stage stochastic optimization problem. We model uncertainties in EV-arrival times and charging demands upon arrival. The model also captures uncertainties in energy prices, non-EV load (which shares the distribution transformer with the charging station), and energy from distributed energy resources (DERs), such as a photovoltaic (PV) solar panel.

To obtain a high-quality solution within the minimum amount of time, we use sample-average approximation (SAA) and an L-shaped method to solve the problem. We also apply the averaged two-replication procedure (A2RP) of Bayraksan and Morton (2011) to control solution quality and the sample sizes in the SAA. Our solution methodology borrows heavily from the work of Bayraksan and Morton (2011). One of the main contributions of our work is that it is the first (to our knowledge) to employ a theoretically valid sampling technique to obtain solutions with statistically valid optimality bounds. Although the solution technique employed is not our own, our use of it to provide robust control of a charging station in real-time is novel.

The remainder of this paper is organized as follows. Section 2 gives an explicit formulation of our station-control model. This model schedules EV charging using a two-stage stochastic optimization framework. It also allows EV charging to be co-optimized with the use of DERs, such as PV and a battery energy storage system (BESS). Section 3 outlines our proposed solution technique, which uses a Monte Carlo-based SAA method to solve the station-control problem and an A2RP to control solution quality and sample sizes. We then demonstrate the use of the model using a case study based on Central Ohio. Section 4 provides detailed case-study data. Case study results are summarized and discussed in Section 5. This includes a comparison of our proposed station-control model to simple heuristics in terms of operation costs, transformer loading and aging, and how much EV-charging demand is unserved. Taking all of these metrics together, our model outperforms the heuristics. We also conduct some sensitivity analyses, in which the design of the charging station or some parameters relating to EV use are varied. This analysis shows the sensitivity of the resulting load profile to different possible EV-usage cases.

The contributions of this work are developing a charging station-control model that captures the unique characteristics of fast charging stations that are not considered in other works in the literature. This includes the ability to model and optimize the use of DERs and capturing uncertainties around EV usage, non-EV load, energy prices, and supply from the DERs. Moreover, we use a Monte Carlo-based SAA technique to efficiently solve the resulting two-stage stochastic program, without having to rely on scenario reduction. Finally, our use of an A2RP allows us to dynamically determine the size of the randomly sampled scenario tree to provide a solution satisfying a desired quality level at minimal computational cost.

## 2. Electric Vehicle Charging Station-Control Model

This section details our EV charging station-control model. The model assumes that the charging station is electrically co-located with a building, with which it shares a distribution-level transformer. This transformer must serve the electrical load of the building, as well as EV-charging loads. The station can also have DERs in the form of a PV plant and a BESS.

There are two types of EVs that arrive to the charging station. The first, which we term inflexible EVs, must have their charging demands met immediately. The others, which we term flexible EVs, have a fixed window of time within which to be recharged. The station-control model determines how to schedule flexible

charging loads and the use of the DERs to meet station load at minimum cost. Our model formulation assumes a one-minute time scale at which control decisions are modeled and made. A one-minute time interval is reasonable for the types of dynamics (*e.g.*, EV arrivals and departures and PV output) modeled.

The station-control model is formulated as a two-stage stochastic optimization problem, which minimizes expected charging station-operation costs over a fixed time horizon. The first stage represents the present time unit (*i.e.*, the next minute), for which here-and-now EV-charging and DER-operational decisions are made. The second stage represents the remainder of the model horizon. The model assumes that the system state (*e.g.*, energy prices, EV and non-EV loads, and PV output) are known for stage one, but that these are uncertain for stage two. A scenario tree represents possible realizations of these random variables in subsequent minutes of the model's time horizon.

Our model determines here-and-now decisions for the next minute only. Our proposed use of this model is in a rolling-horizon fashion. That is to say, the model is used starting from minute $j$ to determine minute-$j$ station-control decisions. The model then rolls forward one minute, updates the stage-one system state and stage-two scenario forecasts, and is re-solved to determine minute-$(j+1)$ decisions. This process repeats to control the charging station. We use the notational convention throughout our formulation that any random parameter with the subscript $t$ is known with certainty at time $t$ (and thereafter) but may be uncertain before time $t$. We use the subscript $\omega$ to represent different second-stage scenarios. We also let the subscript $j$ denote the current minute (*i.e.*, random parameters and decision variables with a $j$ subscript represent known stage-one parameters and here-and-now decisions).

### *2.1. Model Parameters and Functions*

We begin by defining the following model parameters and functions.

| | |
|---|---|
| $\Omega$ | Set of second-stage scenarios |
| $T$ | Optimization horizon [min] |
| $W$ | Charging window for flexible EVs [min] |
| $\bar{H}$ | EV-charger nameplate capacity [kW] |
| $\bar{R}$ | Nameplate transformer capacity [kW] |
| $R^C(\cdot)$ | Penalty for operating transformer above nameplate capacity [$/min] |
| $\bar{S}^{E,+}$ | Maximum state of charge (SOC) of the BESS [kW-min] |
| $\bar{S}^{E,-}$ | Minimum SOC of the BESS [kW-min] |
| $\bar{S}^{P}$ | Charging and discharging capacity of the BESS [kW] |
| $\mu^c$ | Charging efficiency of the BESS |
| $\mu^d$ | Discharging efficiency of the BESS |

Our model has a $T$-minute optimization horizon. The flexible EVs are assumed to have a $W$-minute window of time, within which they must be recharged. We assume that all flexible EVs have the same charging duration for notational brevity. We could, alternately, subdivide the flexible EVs based on the window of time within which they must be recharged. We do not do this, as it would further complicate the model notation.

Each EV is assumed to connect to an $\bar{H}$ kW charger. MW and MWh are typically used as units to measure power and energy, respectively, in electricity systems. We use kW and kW-min throughout our formulation, however. This is because the amount of power transacted in a charging station is on the order of kW and our model has a one-minute temporal granularity.

The charging-station is connected to the electric power system through a distribution transformer, which has a nameplate capacity of $\bar{R}$ kW. As is common utility practice, the transformer can be operated above this nameplate capacity. Doing so has the effect of reducing its usable life. We capture this effect of overloading the transformer through $R^C(\cdot)$, which gives the per-minute cost of overloading the transformer as a function of the amount that the transformer is overloaded (based on the expected loss of transformer life and its replacement cost).

The BESS is represented by its capacity and efficiency in our model. The BESS is assumed to have maximum and minimum SOCs, $\bar{S}^{E,+}$ and $\bar{S}^{E,-}$, respectively. The maximum SOC represents the amount of energy that can be safely stored in the BESS without overloading it. The minimum SOC, which may be nonzero, is modeled because some storage technologies can suffer extreme cycle-life loss if the SOC gets too

low. The BESS also has a power capacity, $\bar{S}^P$, which limits the rate at which it can be charged or discharged. We also assume that energy can be lost when charging or discharging the BESS. The parameters, $\mu^c$ and $\mu^d$, represent these efficiencies. They also implicitly define the cost of storing energy in the BESS (through the energy lost).

### *2.2. State Parameters*

We now define two sets of state parameters. The first, which we term deterministic state parameters, provide all of the system state information up to the current time (*i.e.*, minute $j$). These parameters include exogenous state information (*e.g.*, the minute-$j$ energy price and amount of non-EV and EV-charging loads), as well as decisions that have already been made (*e.g.*, energy that has already been recharged into flexible EVs that arrived before minute $j$). The second, which we term stochastic state parameters, provide possible realizations of the system state in the future (*i.e.*, after minute $j$). Because these parameters represent possible future states of the system (*e.g.*, EV arrivals, PV output, energy prices, and non-EV loads), they are indexed by the second-stage scenarios, $\omega$.

#### *2.2.1. Deterministic State Parameters*

$L_j$ Minute-$j$ inflexible energy demand [kW]

$F_t$ Total charging demand of flexible EVs that arrived to the charging station in minute $t$, where $t \in \{j - W + 1, \ldots, j\}$ [kW-min]

$N_t$ Total number of flexible EVs that arrived to the charging station in minute $t$, where $t \in \{j - W + 1, \ldots, j\}$

$\bar{f}_t$ Total charging demand of flexible EVs that arrived to the charging station in minute $t$, where $t \in \{j - W + 1, \ldots, j\}$, that has been satisfied as of the beginning of minute $j$ [kW-min]

$V_j$ Minute-$j$ PV output [kW]

$p_j$ Minute-$j$ electricity price [\$/kW-min]

$x_j$ Beginning minute-$j$ SOC of the BESS [kW-min]

The charging station faces two types of demands. The first are inflexible demands. These include non-EV demands (*i.e.*, the load of the commercial building sharing the transformer with the charging station) and the charging loads of inflexible EVs. Both of these loads are included in $L_j$.

The second are the demands of flexible EVs. Flexible-EV demands are represented by two parameters. $F_t$ represents the total charging demand of flexible EVs that arrived to the charging station in minute $t$ and $N_t$ represents the total number of EVs that arrived in minute $t$. We assume that the $F_t$ kW-min of charging demand are uniformly spread among the $N_t$ EVs. This assumption is made for notational convenience. We could further subdivide the EVs based on their battery SOC upon arrival to the charging station. Doing so would further complicate the model notation. We let $\bar{f}_t$ denote the total cumulative charging demand of flexible EVs that arrived in minute $t$ that has been satisfied as of the beginning of minute $j$. This is a deterministic state parameter that represents previously made charging-control decisions.

The parameters $F_t$, $N_t$, and $\bar{f}_t$ are defined for values of $t \in \{j - W + 1, \ldots, j\}$. This is because of the assumed $W$-minute charging window. Any EVs that arrived prior to minute $(j - W + 1)$ would no longer be in the station as of minute $j$.

We also define $\xi_j = (L_j, F_t, N_t, \bar{f}_t, V_j, p_j, x_j)$, where $t \in \{j - W + 1, \ldots, j\}$, as the deterministic state-parameter vector.

#### *2.2.2. Stochastic State Parameters*

$L_{t,\omega}$ Minute-$t$ inflexible energy demand in scenario $\omega$ [kW]

$F_{t,\omega}$ Total charging demand of flexible EVs that arrive to the charging station in minute $t$ of scenario $\omega$ [kW-min]

$N_{t,\omega}$ Total number of flexible EVs that arrive to the charging station in minute $t$ of scenario $\omega$

$V_{t,\omega}$ Minute-$t$ PV output in scenario $\omega$ [kW]

$p_{t,\omega}$ Minute-$t$ electricity price in scenario $\omega$ [\$/kW-min]

The stochastic state parameters are all analogous to the deterministic state parameters, except that they are indexed by scenario. This is because the stochastic state parameters represent the second-stage system state, which is unknown when making minute-$j$ here-and-now decisions. We define $\psi_{t,\omega} = (L_{t,\omega}, F_{t,\omega}, N_{t,\omega}, V_{t,\omega}, p_{t,\omega})$ as a vector of scenario-$\omega$ minute-$t$ stochastic state parameters. We also define $\psi_\omega = (\psi_{j+1,\omega}, \ldots, \psi_{j+T,\omega}) \in \Psi$ as the scenario-$\omega$ sample path of stochastic state parameters.

### *2.3. Decision Variables*

We define two sets of decision variables: those corresponding to first- and second-stage decisions.

#### *2.3.1. First-Stage Decision Variables*

| | |
|---|---|
| $e_j^s$ | Minute-$j$ power sales to the power system [kW] |
| $e_j^b$ | Minute-$j$ power purchases from the power system [kW] |
| $e_j^c$ | Minute-$j$ power charged into the BESS [kW] |
| $e_j^d$ | Minute-$j$ power discharged from the BESS [kW] |
| $x_{j+1}$ | Beginning minute-$(j+1)$ SOC of battery energy storage [kW-min] |
| $f_{j,\tau}$ | Total kW provided in minute $j$ to recharge flexible EVs that arrived to the charging station in minute $\tau$, where $\tau \in \{j-W+1, \ldots, j\}$ [kW] |
| $f_j$ | Total kW provided in minute $j$ to recharge flexible EVs [kW] |
| $v_j$ | Minute-$j$ transformer overload [kW] |

The first-stage decision variables pertain to the minute-$j$ here-and-now decisions. The first pair of variables, $e_j^s$ and $e_j^b$, represent energy transacted between the charging station and the power system. Depending on local demand and energy production from the DERs, the charging station may purchase energy from or sell energy to the power system (in net) at a given point in time. These transactions are settled at the energy price, $p_j$.

The variables, $e_j^c$ and $e_j^d$, represent BESS charging and discharging decisions and $x_{j+1}$ represents the resulting beginning minute-$(j+1)$ SOC of the BESS. We let $f_{j,\tau}$ denote the amount of charging load provided to flexible EVs that arrived to the charging station in minute $\tau$ and $f_j$ the sum of the $f_{j,\tau}$'s.

We also define $a_j = (e_j^s, e_j^b, e_j^c, e_j^d, x_{j+1}, f_{j,\tau}, f_j, v_j)$, where $\tau \in \{j-W+1, \ldots, j\}$ as the first-stage decision-variable vector.

#### *2.3.2. Second-Stage Decision Variables*

| | |
|---|---|
| $e_{t,\omega}^s$ | Minute-$t$ power sales to the power system in scenario $\omega$ [kW] |
| $e_{t,\omega}^b$ | Minute-$t$ power purchases from the power system in scenario $\omega$ [kW] |
| $e_{t,\omega}^c$ | Minute-$t$ power charged into the BESS in scenario $\omega$ [kW] |
| $e_{t,\omega}^d$ | Minute-$t$ power discharged from the BESS in scenario $\omega$ [kW] |
| $x_{t+1,\omega}$ | Beginning minute-$(t+1)$ SOC of the BESS in scenario $\omega$ [kW-min] |
| $f_{t,\tau,\omega}$ | Total kW provided in minute $t$ of scenario $\omega$ to recharge flexible EVs that arrived to the charging station in minute $\tau$ [kW] |
| $f_{t,\omega}$ | Total kW provided in minute $t$ of scenario $\omega$ to recharge flexible EVs [kW] |
| $v_{t,\omega}$ | Minute-$t$ transformer overload in scenario $\omega$ [kW] |

The second-stage decision variables are analogous to the first-stage decision variables, except that they represent second-stage recourse decisions. As such, the second-stage variables are all indexed by the second-stage scenarios, $\omega$. We define $u_{t,\omega} = (e_{t,\omega}^s, e_{t,\omega}^b, e_{t,\omega}^c, e_{t,\omega}^d, x_{t+1,\omega}, f_{t,\tau,\omega}, f_{t,\omega}, v_{t,\omega})$ as the scenario-$\omega$/minute-$t$ second-stage decision-variable vector. We also define $u_\omega = (u_{j+1,\omega}, \ldots, u_{j+T,\omega})$ as the scenario-$\omega$ second-stage decision-variable vector.

### *2.4. Constraints*

We define two types of problem constraints: first- and second-stage constraints. In the first stage, we first have a power-balance constraint:

$$L_j + f_j + e_j^c = V_j + e_j^d + e_j^b - e_j^s. \tag{1}$$

This constraint ensures that power consumed within the charging station for serving inflexible or flexible loads or charging the BESS equals the sum of power produced by the PV system, discharged from the BESS, or transacted with the power system. We next have constraints:

$$v_j + \bar{R} \geq e_j^b - e_j^s; \tag{2}$$

and:

$$-v_j - \bar{R} \leq e_j^b - e_j^s; \tag{3}$$

imposing the transformer's capacity. These constraints restrict net power transactions with the power system, $(e_j^b - e_j^s)$, based on the transformer capacity, $\bar{R}$. The constraint allows the transformer to operate above its capacity, in which case $v_j$ must take on a positive value.

We next have an energy-balance constraint defining the evolution of the BESS SOC:

$$x_{j+1} = x_j + \mu^c \cdot e_j^c - e_j^d/\mu_d; \tag{4}$$

bounds on the BESS SOC:

$$\bar{S}^{E,-} \leq x_{j+1} \leq \bar{S}^{E,+}; \tag{5}$$

and power limits on charging and discharging:

$$e_j^c, e_j^d \leq \bar{S}^P. \tag{6}$$

The next set of constraints involve flexible-EV recharging. We first have constraints:

$$f_{j,\tau} \leq \bar{H} \cdot N_\tau; \forall \tau = j - W + 1, \ldots, j; \tag{7}$$

which restrict the total amount that flexible EVs that arrived in minute $\tau$ can be recharged based on the charger capacity and the total number of EVs. We next have a constraint defining the total amount that flexible EVs are recharged in minute $j$:

$$f_j = \sum_{\tau=j-W+1}^{j} f_{j,\tau}. \tag{8}$$

We also have sets of constraints that ensure that none of the flexible EVs are over- or undercharged. The first:

$$f_{j,\tau} \leq F_\tau - \bar{f}_\tau; \forall \tau = j - W + 1, \ldots, j; \tag{9}$$

restricts the amount recharged in EVs that arrived in minute $\tau$ to be no greater than the remaining unfulfilled charging demand as of the beginning of minute $j$. The second:

$$F_\tau - \bar{f}_\tau - f_{j,\tau} \leq \bar{H} \cdot N_\tau \cdot (W - j + \tau - 1); \forall \tau = j - W + 1, \ldots, j; \tag{10}$$

ensures that the remaining unfulfilled charging demand (as of the end of minute $j$) of EVs that arrived in minute $\tau$ could be feasibly met if they are recharged at the charger's maximum capacity for the remainder of the charging window.

We finally have non-negativity constraints:

$$e_j^s, e_j^b, e_j^c, e_j^d, x_{j+1}, f_j, v_j \geq 0; \tag{11}$$

and:

$$f_{j,\tau} \geq 0, \forall \tau = j - W + 1, \ldots, j. \tag{12}$$

The second-stage constraints have a very similar structure, in that they impose the same sets of restrictions. The major difference between the first- and second-stage constraints is that the second-stage constraints are scenario-dependent. We define the scenario-$\omega$ second-stage constraints here. We first have a set of power-balance constraints:

$$L_{t,\omega} + f_{t,\omega} + e_{t,\omega}^c = V_{t,\omega} + e_{t,\omega}^d + e_{t,\omega}^b - e_{t,\omega}^s; \forall t = j + 1, \ldots, j + T. \tag{13}$$

We next have transformer-capacity constraints:

$$v_{t,\omega} + \bar{R} \geq e^b_{t,\omega} - e^s_{t,\omega}; \forall t = j+1, \ldots, j+T. \tag{14}$$

and:

$$-v_{t,\omega} - \bar{R} \leq e^b_{t,\omega} - e^s_{t,\omega}; \forall t = j+1, \ldots, j+T. \tag{15}$$

Next are constraints for the BESS. The constraint sets:

$$x_{j+2,\omega} = x_{j+1} + \mu^c \cdot e^c_{j+1,\omega} - e^d_{j+1,\omega}/\mu^d; \tag{16}$$

and:

$$x_{t+1,\omega} = x_{t,\omega} + \mu^c \cdot e^c_{t,\omega} - e^d_{t,\omega}/\mu^d; \forall t = j+2, \ldots, j+W; \tag{17}$$

define the evolution of the BESS SOC in each minute. Constraint sets:

$$\bar{S}^{E,-} \leq x_{t,\omega} \leq \bar{S}^{E,+}; \forall t = j+2, \ldots, j+W+1; \tag{18}$$

and:

$$e^c_{t,\omega}, e^d_{t,\omega} \leq \bar{S}^P; \forall t = j+2, \ldots, j+W; \tag{19}$$

impose the SOC and charging and discharging power limits of the BESS, respectively.

We next have constraints related to flexible-EV charging. The first set imposes the chargers' capacities:

$$f_{t,\tau,\omega} \leq \bar{H} \cdot N_{\tau,\omega}; \forall t = j+1, \ldots, j+T; \tau = t-W+1, \ldots, t; \tag{20}$$

and the second defines total flexible-EV charging in each minute of each scenario:

$$f_{t,\omega} = \sum_{\tau=t-W+1}^{t} f_{t,\tau,\omega}; \forall t = j+1, \ldots, j+T. \tag{21}$$

We finally need additional sets of constraints to ensure that all of the flexible EVs are recharged. First, we ensure that all vehicles that have already arrived as of minute $j$ will be fully recharged within the charging window under all scenarios:

$$\sum_{t=j+1}^{\tau+W} f_{t,\tau,\omega} + f_{j,\tau} = F_\tau - \bar{f}_\tau; \forall \tau = j-W+1, \ldots, j. \tag{22}$$

Next, we ensure that all flexible EVs that arrive after minute $j$ and that have a charging window that ends before the $T$-minute model horizon are fully recharged:

$$\sum_{t=\tau}^{\tau+W} f_{t,\tau,\omega} = F_\tau; \forall \tau = j+1, \ldots, j+T-W. \tag{23}$$

We finally ensure that the remaining EVs (*i.e.*, those that will arrive after minute $j$ but have a charging window that ends after the $T$-minute model horizon) are not overcharged but have been charged sufficiently to be able to recharge before their charging windows expire. These constraint sets are written as:

$$\sum_{t=\tau}^{j+T} f_{t,\tau,\omega} \leq F_\tau; \forall \tau = j+T-W+1, \ldots, j+T; \tag{24}$$

and:

$$F_\tau - \sum_{t=\tau}^{j+T} f_{t,\tau,\omega} \leq \bar{H} \cdot N_{\tau,\omega} \cdot (W-j-T+\tau); \forall \tau = j+T-W+1, \ldots, j+T. \tag{25}$$

We finally have non-negativity constraints:

$$e^s_{t,\omega}, e^b_{t,\omega}, e^c_{t,\omega}, e^d_{t,\omega}, x_{t+1,\omega}, f_{t,\omega}, v_{t,\omega} \geq 0; \forall t = j+1, \ldots, j+T; \tag{26}$$

and:

$$f_{t,\tau,\omega} \geq 0; \forall t = j+1, \ldots, j+T; \tau = t-W+1, \ldots, t. \tag{27}$$

For notional convenience, we also define the first-stage feasible region as:

$$A_j = \{a_j | \, (1)\text{–}(12)\}.$$

We similarly define the second-stage feasible region on sample path $\omega$ as:

$$U_\omega = \{u_\omega | \, (13)\text{–}(27)\}.$$

We finally note that (10) ensures that this problem has relatively complete recourse. These constraints ensure that all of the EVs that are in the charging station as of minute $j$ are charged sufficiently so that they could be fully recharged within the $W$-minute charging window.

### *2.5. Objective Function*

To define the objective function, we begin by defining the minute-$j$ charging station-operation cost as:

$$c_j(a_j, \xi_j) = p_j \cdot (e^b_j - e^s_j) + R^C(v_j). \tag{28}$$

The first term in (28) gives the cost of energy transacted with the power system, while the second term represents the cost of overloading the distribution-level transformer. We similarly define the second-stage cost in minute $t$ of scenario $\omega$ as:

$$c_{t,\omega}(u_{t,\omega}, \psi_{t,\omega}) = p_{t,\omega} \cdot (e^b_{t,\omega} - e^s_{t,\omega}) + R^C(v_{t,\omega}).$$

The two terms in this function have the same interpretations as those in (28). The charging station-control problem is then formulated as:

$$\min_{a_j \in A_j} \{g(a_j) = c_j(a_j, \xi_j) + \mathbb{E}\left[r(a_j, \psi_\omega)\right]\}, \tag{29}$$

where we define:

$$r(a_j, \psi_\omega) = \min_{u_\omega \in U_\omega} \sum_{t=j+1}^{j+T} c_{t,\omega}(u_{t,\omega}, \psi_{t,\omega}). \tag{30}$$

Objective function (29) minimizes the sum of the stage-one cost, which is the first term, and the expected second-stage cost, which is the second term. The second-stage is cost is defined by (30) as the sum of costs accumulated in each of minutes $(j+1)$ through $(j+T)$.

## 3. Solution Technique

First-stage objective function (29) is implicitly defined by the second-stage problems. As such, all of the second-stage problems must be solved to obtain an optimal solution to the station-control problem. The second-stage problems are defined by forecasting second-stage scenarios through the end of the $T$-minute model horizon. These second-stage scenarios are defined by different realizations of the second-stage parameter vector, $\psi_\omega$. Some of the second-stage parameters are continuous random variables, implying that there are an infinite number of second-stage parameter vectors and, as such, an infinite number of second-stage problems.

These properties of the station-control problem make it computationally challenging. Our proposed use of the station-control problem is in a rolling-horizon fashion, whereby it is re-solved every minute. Thus,

the station-control problem must be solved quickly. To accomplish this, we apply a SAA approach to quickly obtain near-optimal solutions within seconds. We also apply a sequential sampling procedure (SSP) proposed by Bayraksan and Morton (2011) to estimate and control the quality of the solutions obtained from the SAA.

We proceed in this section by first defining the SAA problem and then detailing the algorithm used to solve it. We next discuss the gap and variance estimators used to assess the quality of a solution given by the SAA problem and determine the stopping criterion for our solution algorithm. We finally discuss the convergence properties of our solution method.

### *3.1. Sample Average Approximation Problem*

An SAA problem replaces the infinite number of second-stage problems that define the true station-control problem with a finite random sample of second-stage scenarios. We solve the SAA problem in an iterative fashion, in which the number of second-stage scenarios sampled is increased until the solution to the SAA problem satisfies a desired termination criterion.

To formulate the SAA problem, we first define $\psi_1, \ldots, \psi_{m_\kappa}$ as $m_\kappa$ independent and identically distributed (i.i.d.) samples of the second-stage sample paths (*i.e.*, samples of $\psi_\omega$). The $\kappa$ subscript on $m_\kappa$ denotes the iteration number of the algorithm employed to solve the SAA problem (*cf.* Algorithm 1). The samples, $\psi_1, \ldots, \psi_{m_\kappa}$, are randomly generated by a Monte Carlo simulation. The method used to generate the sequence of $m_\kappa$'s is further discussed in Section 3.4 (*cf.* Equation (39) in particular) and all of the $m_\kappa$'s are integral. The SAA problem is formulated as:

$$\min_{a_j \in A_j} \left\{ g^{m_\kappa}(a_j) = \frac{1}{m_\kappa} \sum_{m=1}^{m_\kappa} \left[ c_j(a_j, \xi_j) + r(a_j, \psi_m) \right] \right\}; \tag{31}$$

where we define:

$$r(a_j, \psi_m) = \min_{u_m \in U_m} \sum_{t=j+1}^{j+T} c_{t,m}(u_{t,m}, \psi_{t,m}). \tag{32}$$

Algorithm 1 provides a high-level overview of the method used to solve the SAA problem. Step 1 begins by choosing sample-size sequences, $\{m_\kappa\}$ and $\{l_\kappa\}$, and a termination criterion, $\Upsilon$ (*cf.* Sections 3.3 and 3.4). The sample-size sequence, $\{l_\kappa\}$, is used to estimate the optimality gap of the solution to the SAA problem solved in each iteration. Steps 3–8 are the main iterative loop. In Step 4 of iteration $\kappa$, the $m_\kappa$ i.i.d. random samples are generated to define an SAA problem. This problem is solved using an L-shaped method (*cf.* Section 3.2) in Step 5. In Step 6, $l_\kappa$ i.i.d. samples of the random variables are generated to estimate the optimality gap of the solution to the SAA problem found in Step 5. This gap estimator is used in the termination criterion (*cf.* Sections 3.3 and 3.4). The iterative process repeats, with the sample size of the SAA problems increasing, until stopping criterion $\Upsilon$, is satisfied.

**Algorithm 1** SAA Method

1: **input:** sample-size sequences $\{m_\kappa\}$ and $\{l_\kappa\}$, stopping criterion $\Upsilon$
2: $\kappa \leftarrow 0$
3: **repeat**
4: generate $m_\kappa$ i.i.d. random samples, $\psi_1, \ldots, \psi_{m_\kappa}$ of second-stage sample path
5: solve SAA problem (31) using L-shaped method
6: generate $l_\kappa$ i.i.d. random samples and optimality gap estimator
7: $\kappa \leftarrow \kappa + 1$
8: **until** $\Upsilon$ is satisfied

The following subsections provide further details of the L-shaped method (*cf.* Step 5) and the selection of the sample-size sequences and stopping criterion (*cf.* Step 1).

*3.2. Solution of SAA method*

We use an L-shaped method to solve the SAA problem in Step 5 of Algorithm 1. This method works by doing a Benders-type decomposition of (31). We define the master problem:

$$\min_{a_j \in A_j, \theta} \frac{1}{m_\kappa} \sum_{m=1}^{m_\kappa} [c_j(a_j, \xi_j) + \theta_m]\,; \tag{33}$$

where $\theta_1, \ldots, \theta_{m_\kappa}$ is a set of new variables. The variable, $\theta_m$, is an estimate of the second-stage objective-function value under sample path $\psi_m$. Thus, $\theta_m$ is estimating $r(a_j, \psi_m)$.

Problem (33) relaxes the optimality of the second-stage decisions, which is required to solve (31). Thus, any optimal solution of (33) should be checked to verify whether it satisfies or violates second-stage optimality. If one of the $\theta_m$'s violates this optimality, *i.e.*, if:

$$\theta_m < r(a_j, \psi_m);$$

for some $m$, then an optimality cut should be added to (33). These optimality cuts are obtained from the optimal solution of the dual of (32). More specifically, let $\pi_m$ and $\Pi_m$ denote the variable vector and feasible region, respectively, of the dual of the sample path-$m$ second-stage problem. The dual of (32) can then be written as:

$$\max_{\pi_m \in \Pi_m} \phi(\pi_m, a_j, \psi_m). \tag{34}$$

Note that $\phi(\pi_m, a_j, \psi_m)$ is the optimal objective-function value of the sample path-$m$ second-stage problem with first-stage decision-variable values, $a_j$. Because of strong duality, $r(a_j, \psi_m)$ is equal to the optimal objective-function value of (34). Thus, the separated optimality cuts are:

$$\theta_m \geq \phi(\pi_m^*, a_j, \psi_m); \tag{35}$$

where $\pi_m^*$ is the optimal dual-variable vector of (34).

Benders's-type decomposition schemes typically also require adding feasibility cuts to the master problem. This is because master problem (33) relaxes feasibility of the second-stage problems (*i.e.*, first-stage decisions are made without explicit consideration of second-stage constraints). Feasibility cuts are not necessary for our problem, however, because (10) guarantees that Problem (29) has relatively complete recourse. Because Constraints (10) are imposed in master problem (33) as well (it is minimizing over the same first-stage feasible set, $A_j$), feasibility cuts are not necessary.

The L-shaped method iteratively adds optimality cuts to master problem (33). To more explicitly specify this iterative technique, we first define the L-shaped master SAA problem. To do this, we let $K_1, \ldots, K_{m_\kappa}$ denote the number of optimality cuts that have already been added to the problem for each of sample paths, $\psi_1, \ldots, \psi_{m_\kappa}$, respectively. We also let $\pi_m^k$ denote the optimal dual vector, which is obtained from (34), to generate the $k$th optimality cut for sample path $m$. The L-shaped master SAA problem is then given by:

$$\min_{a_j, \theta} \frac{1}{m_\kappa} \sum_{m=1}^{m_\kappa} [c_j(a_j, \xi_j) + \theta^m] \tag{36}$$

$$\text{s.t.} \quad a_j \in A_j;$$

$$\theta^m \geq \phi(\pi_m^k, a_j, \psi_m); \qquad \forall m = 1, \ldots, m_\kappa; k = 1, \ldots, K_m. \tag{37}$$

For notational convenience, we define the feasible region of the L-shaped master problem as:

$$\tilde{A}_j = \{(a_j, \theta) \in A_j \times \mathbb{R}^{m_\kappa} | \, (37)\}\,.$$

Algorithm 2 outlines the L-shaped method. The set of optimality cuts is first initialized to be empty in Step 1. In Step 3, the incumbent master problem is solved to obtain the solution, $(\hat{a}_j, \hat{\theta})$. We then iterate through each second-stage sample path and solve the cut-separation problem in Step 5. If, in Step 6, we find that the value of $\hat{\theta}_m$ underestimates the true second-stage objective-function value, $\phi(\hat{\pi}_m, \hat{a}_j, \psi_m)$, then a new sample path-$m$ optimality cut is added in Steps 7 and 8. This iterative procedure repeats until $\hat{\theta}$ does not underestimate the true second-stage objective-function value of any sample path.

**Algorithm 2** L-Shaped method for SAA Problem

$K_m \leftarrow 0, \forall m = 1, \ldots, m_\kappa$
**repeat**
  $(\hat{a}_j, \hat{\theta}) \leftarrow \arg \min_{(a_j,\theta)\in \tilde{A}_j}$ (36)
  **for** $m = 1, \ldots, m_\kappa$ **do**
    $\hat{\pi}_m \leftarrow \arg \max_{\pi_m \in \Pi_m}$ (34)
    **if** $\phi(\hat{\pi}_m, \hat{a}_j, \psi_m) > \hat{\theta}^m$ **then** ▷ add a new sample path-$m$ optimality cut
      $K_m \leftarrow K_m + 1$
      $\pi_m^{K_m} \leftarrow \hat{\pi}_m$
    **end if**
  **end for**
**until** $\frac{1}{m_\kappa} \sum_{m=1}^{m_\kappa} \hat{\theta}_m \geq \frac{1}{m_\kappa} \sum_{m=1}^{m_\kappa} r(\hat{a}_j, \psi_m)$

### *3.3. Gap and Variance Estimators*

The termination criterion, $\Upsilon$, in Algorithm 1 requires us to assess the quality of the solution found in Step 5. We do this by applying SSP with A2RP. More specifically, SSP gives gap and variance estimators using the optimality-gap estimators provided by the A2RP. We first introduce the gap and variance estimates provided by the A2RP.

A2RP is a batch-mean-based method suggested by Bayraksan and Morton (2006). We begin by defining $g^*$ to be the optimal objective value of the original problem:

$$g^* = \min_{a_j \in A_j} g(a_j);$$

where $g(a_j)$ is defined in (29). We also let:

$$A^* = \{a_j \in A_j | g(a_j) = g^*\};$$

denote the set of optimal solutions of (29). We similarly define $\hat{g}^{m_\kappa}$ as the optimal objective-function value of SAA problem (31) with $m_\kappa$ randomly generated sample paths:

$$\hat{g}^{m_\kappa} = \min_{a_j \in A_j} g^{m_\kappa}(a_j);$$

and $\hat{A}^{m_\kappa}$ as the corresponding optimal-solution set:

$$\hat{A}^{m_\kappa} = \{a_j \in A_j | g^{m_\kappa}(a_j) = \hat{g}^{m_\kappa}\}.$$

The optimality gap and gap variance are defined, respectively, as:

$$\mu(a_j) = g(a_j) - g^*;$$

and:

$$\sigma^2(a_j) = \mathrm{Var}\left(r(a_j, \psi_\omega) - r(a_j^*, \psi_\omega)\right);$$

where $a_j^* \in A^*$.

A2RP compares an optimal solution obtained from solving the SAA problem with the $m_\kappa$ random sample paths in Step 5 of Algorithm 1, to an optimal solution obtained from solving an SAA problem with a different set of stochastic parameters. We only provide an outline of the A2RP method here and refer interested readers to the work of Bayraksan and Morton (2006) for further details.

We begin by defining two new randomly generated sample paths, $\dot{\psi}_1^1, \ldots, \dot{\psi}_1^{l_\kappa/2}$ and $\dot{\psi}_2^1, \ldots, \dot{\psi}_2^{l_\kappa/2}$, each of size $l_\kappa/2$. The optimality-gap estimators are then defined as:

$$G^i_{l_\kappa/2}(a_j^{m_\kappa *}) = g^{l_\kappa/2,i}(a_j^{m_\kappa *}) - \min_{a_j \in A_j} g^{l_\kappa/2,i}(a_j); \forall i = 1, 2;$$

where $a_j^{m_\kappa *}$ is the optimal solution from Step 5 of Algorithm 1 (*i.e.*, $a_j^{m_\kappa *} \in \hat{A}^{m_\kappa}$) and $g^{l_\kappa/2,i}(\cdot)$ is defined by (31) with the parameter $m_\kappa$ on the right-hand side replaced with $l_\kappa/2$. Note that:

$$g^{l_\kappa/2,i}(a_j) = c_j(a_j, \xi_j) + \frac{2}{l_\kappa} \sum_{l=1}^{l_\kappa/2} r(a_j, \dot{\psi}_i^l).$$

We also define:

$$a_j^{l_\kappa/2,i^*} = \arg\min_{a_j \in A_j} g^{l_\kappa/2,i}(a_j);$$

as the minimizer of the second term defining $G^i_{l_\kappa/2}(a_j^{m_\kappa *})$. Thus, we can write:

$$G^i_{l_\kappa/2}(a_j^{m_\kappa *}) = g^{l_\kappa/2,i}(a_j^{m_\kappa *}) - g^{l_\kappa/2,i}(a_j^{l_\kappa/2,i^*}); \forall i = 1, 2.$$

The variance estimators of the optimality gaps are defined as:

$$s^2_{l_\kappa/2}(a_j^{l_\kappa/2,i^*}) = \frac{2}{l_\kappa - 2} \sum_{l=1}^{l_\kappa/2} \left\{ \left[ \left( c_j(a_j^{m_\kappa *}, \xi_j) + r(a_j^{m_\kappa *}, \dot{\psi}_i^l) \right) - \left( c_j(a_j^{l_\kappa/2,i^*}, \xi_j) + r(a_j^{l_\kappa/2,i^*}, \dot{\psi}_i^l) \right) \right] - G^i_{l_\kappa/2}(a_j^{m_\kappa *}) \right\}^2;$$

for all $i = 1$ and 2. The mean and variance estimates are calculated as:

$$\bar{G}_{l_\kappa/2}(a_j^{m_\kappa *}) = \frac{1}{2} \left[ G^1_{l_\kappa/2}(a_j^{m_\kappa *}) + G^2_{l_\kappa/2}(a_j^{m_\kappa *}) \right];$$

and:

$$\bar{s}^2_{l_\kappa}(a_j^{m_\kappa *}) = \frac{1}{2} \left[ s^2_{l_\kappa/2}(a_j^{l_\kappa/2,1^*}) + s^2_{l_\kappa/2}(a_j^{l_\kappa/2,2^*}) \right].$$

### *3.4. Stopping Criterion and Sample Sizes*

We use an SSP stopping criterion proposed by Bayraksan and Morton (2011). We denote the stopping criterion as $\Upsilon$. $\Upsilon$ should ensure that the algorithm provides a high-quality solution in a finite number of iterations. The stopping criterion, $\Upsilon$, is defined as:

$$\bar{G}_{l_\kappa/2}(a_j^{m_\kappa *}) \leq h' \bar{s}_{l_\kappa}(a_j^{m_\kappa *}) + \epsilon'; \tag{38}$$

where $h' > 0$ is a relative tolerance and $\epsilon' > 0$ ensures finite stopping. We define the first iteration that satisfies $\Upsilon$ as:

$$\Gamma = \inf_{\kappa \geq 1} \left\{ \kappa \,\middle|\, \bar{G}_{l_\kappa/2}(a_j^{m_\kappa *}) \leq h' \bar{s}_{l_\kappa}(a_j^{m_\kappa *}) + \epsilon' \right\}.$$

Stopping criterion (38) requires that the optimality gap, $\bar{G}_{l_\kappa/2}(a_j^{m_\kappa *})$, be no more than a fraction, $h'$, of its standard deviation, $\bar{s}_{l_\kappa}(a_j^{m_\kappa *})$. Criterion (38) is satisfied with probability 1 if $l_\kappa < +\infty$, $m_\kappa < +\infty$, and $\epsilon' > 0$. In fact, $\epsilon'$ limits the order of magnitude of the optimality gap when the algorithm terminates. For instance, the algorithm terminates if $\bar{G}_{l_\kappa/2}(a_j^{m_\kappa *}) = 10^{-8}$ and $\epsilon' = 10^{-7}$ no mater what value $\bar{s}_{l_\kappa}(a_j^{m_\kappa *})$ takes. Thus, $\epsilon'$ should be appropriately small to avoid interfering with Algorithm 1 stopping when the optimality gap and the corresponding standard deviation are large. For further details of finite stopping with positive $\epsilon'$, we refer interested readers to the work of Bayraksan and Morton (2011).

Stopping criterion (38) is defined in terms of parameters $h'$ and $\epsilon'$. However, the confidence interval on the optimality gap, once the stopping criterion is satisfied, is actually given in terms of:

$$h \cdot \bar{s}_{l_\kappa}(a_j^{m_\Gamma *}) + \epsilon;$$

where $h > h'$ and $\epsilon > \epsilon'$. The reason that the confidence interval is inflated (*i.e.*, is given in terms of $h$ and $\epsilon$ as opposed to $h'$ and $\epsilon'$) is because of the sequential nature of the sampling method employed. We choose the sample-size sequence, $\{m_\kappa\}$, such that:

$$m_\kappa \geq \left(\frac{1}{h - h'}\right)^2 \left(\eta_q + 2q \cdot [\log(\kappa)]^2\right); \tag{39}$$

where:

$$\eta_q = \max\left\{2\log\left(\frac{\sum_{\iota=1}^{+\infty} \iota^{-q\log\iota}}{\sqrt{2\pi}\alpha}\right), 1\right\};$$

$(1-\alpha)$ is the desired confidence level of the confidence interval obtained, with $\alpha \in (0,1)$, and $q > 0$ is a parameter that governs the sample sizes. The value of $q$ is chosen to minimize the computational effort, which is defined by the total number of samples required in Algorithm 1 (*i.e.*, $\sum_{\kappa=1}^{\Gamma} m_\kappa$). Further details on the choice of $q$ are provided by Bayraksan and Morton (2011).

Algorithm 3 outlines the procedure employed to determine the stopping criterion and the sample-size sequence. For notational convenience, we define $\Delta h = h - h'$ and $\Delta\epsilon = \epsilon - \epsilon'$. The algorithm takes two inputs in Step 1—an initial sample size, $m_0$, and a desired number of iterations, $\Gamma_0$, for Algorithm 1. These inputs are used to determine $\Upsilon$ and $\{m_\kappa\}$. $\Gamma_0$ represents a tradeoff between the amount of computational work involved in solving the station-control problem and the tightness of the confidence interval on the optimality gap obtained. A higher value of $\Gamma_0$ tightens the confidence interval but also increases:

$$\sum_{\kappa=1}^{\Gamma_0} m_\kappa;$$

the number and size of the SAA problems that must be solved. Step 4 calculates $\eta_q$. In practice, the:

$$\sum_{\iota=1}^{+\infty} \iota^{-q\log\iota}; \tag{40}$$

term is approximated by replacing $+\infty$ in the upper limit of the sum with a large but finite number. Note that (40) converges to a finite value because $q > 0$.

In Steps 6–9 we generate and solve $\rho$ SAA problems with sample sizes of $m_0$. The results of these initial SAA problems are used to generate a set of gap and variance estimates, which are averaged in Steps 10 and 11. These average gap and variance estimates are used in Step 12 to determine $h'$. The reasoning behind choosing $h'$ in this way is that the initial $\rho$ SAA problems give us a sense of the ratio between the optimality gap and its variance for near-optimal solutions. $\bar{\mathcal{G}}$ and $\bar{f}$ are random samples of these two values. Thus, we use $\bar{\mathcal{G}}$ and $\bar{f}$ to determine $h'$. Indeed, $h'$ specifies the instance stochasticity and $h' \propto \bar{\mathcal{G}}/\bar{f}$. The reason for solving multiple SAA problems is to avoid a biased set of samples and to estimate the average uncertainty using a set of near-optimal solutions. Values of $\rho$ between 2 and 5 are common and we use $\rho = 2$. $\beta$ is a user-specified positive relative stopping constant and is usually fixed between 0.9 and 1. We use $\beta = 1$. In this setting, the tightness of stopping criterion (38) is decided by the variance of the objective function around the optimal solution. For instance, criterion (38) is tight if the variance is small. Otherwise, a relatively loose stopping criterion is given.

The values of $\epsilon'$ and $\epsilon$ are fixed in Steps 14 and 15. In practice, these two parameters can be set to any reasonable positive numbers, based on observed behavior of the optimality and variance of the problem being

**Algorithm 3** Stopping Criterion and Sample Sizes Initialization

1: **input:** $m_0$ and $\Gamma_0$ ▷ $m_0$: initial sample size, $\Gamma_0$: desired iterations
2: $l_0 \leftarrow 2 \cdot \lceil m_0/2 \rceil$
3: choose $q$ based on $\Gamma_0$ ▷ *cf.* Bayraksan and Morton (2011)
4: $\eta_q \leftarrow \max\{2\log(\sum_{\iota=1}^{+\infty} \iota^{-q\log\iota}/\sqrt{2\pi}\alpha), 1\}$
5: $\Delta h \leftarrow \sqrt{\frac{\eta_q}{m_0}}$ ▷ based on (39) with $\kappa = 1$
6: **for** $\varrho = 1, \ldots, \rho$ **do**
7: solve (31) with $m_0$ second-stage sample paths using Algorithm 2 ▷ let $a_j^{m_0^{\varrho}*}$ denote solution
8: solve A2RP problems to obtain $\bar{G}_{l_\kappa/2}(a_j^{m_0^{\varrho}*})$ and $\bar{s}^2(a_j^{m_0^{\varrho}*})$
9: **end for**
10: $\bar{\mathcal{G}} \leftarrow \frac{1}{\rho}\sum_{\varrho=1}^{\rho} \bar{G}_{l_\kappa/2}(a_j^{m_0^{\varrho}*})$
11: $\bar{f}^2 \leftarrow \frac{1}{\rho}\sum_{\varrho=1}^{\rho} \bar{s}^2_{l_\kappa}(a_j^{m_0^{\varrho}*})$
12: $h' \leftarrow \beta \cdot (\bar{\mathcal{G}}/\bar{f})$
13: $h \leftarrow h' + \Delta h$
14: $\epsilon' \leftarrow 1 \times 10^{-7}$
15: $\epsilon \leftarrow 2 \times 10^{-7}$
16: generate $\{m_\kappa\}$ using (39)
17: $l_\kappa \leftarrow 2 \cdot \lceil m_\kappa/2 \rceil, \forall k$
18: **output:** $h', h, \epsilon'$, $\epsilon$, $\{m_\kappa\}$, and $\{l_\kappa\}$

solved. Finally, the sample-size sequences, $\{m_\kappa\}$ and $\{l_\kappa\}$, are generated in Steps 16 and 17, using (39). We generate the $m_\kappa$'s as:

$$m_\kappa \leftarrow \left\lceil \left(\frac{1}{h - h'}\right)^2 \left(\eta_q + 2q \cdot [\log(\kappa)]^2\right) \right\rceil.$$

A consequence of using the sample sizes and stopping criterion found in Algorithm 3 is that:

$$[0, h \cdot \bar{s}_{l_\kappa}(a_j^{m_\Gamma *}) + \epsilon];$$

is a valid $(1-\alpha)$ confidence interval on the optimality gap, so long as $\Delta h$ has order of magnitude less than $\Delta\epsilon/\mathcal{M}$, where $\mathcal{M}$ is the supremum of the optimality gap's variance. Further details regarding the asymptotic validity of the stopping criterion are given in Section 3.6.

### *3.5. Convergence Properties of SAA*

An important question in applying Algorithm 1 is whether there are any guarantees that SAA problem (31) converges to the true station-control problem given by (29). Convergence of the SAA problem relies on the results of Shapiro et al. (2014). Before answering this question, we first place an additional assumption on the stochastic properties of the station-control problem and show four additional properties of the original and SAA problems. These are then used to appeal to a theorem shown by Shapiro et al. (2014), which provides our convergence result.

**Assumption 1.** *$p_{t,\omega}$ has a finite moment-generating function (MGF). Moreover, random vectors $V_{t,\omega}$, $L_{t,\omega}$, $N_{t,\omega}$ and $F_{t,\omega}$ are all bounded.*

The assumption on the MGF of $p_{t,\omega}$ says that there exists a $\gamma_0 > 0$ such that for all $\gamma \in (-\gamma_0, \gamma_0)$ we have that $M(\gamma)$ is finite, where:

$$M(\gamma) = \mathbb{E}\left[e^{\gamma \cdot p_{t,\omega}}\right] < +\infty;$$

is the MGF of $p_{t,\omega}$.

We now show the additional properties of the original and SAA problems through the following lemma and propositions.

**Lemma 1.** *Suppose that there exist $N$ independent random variables, $X_1, X_2, \ldots, X_N$, for some $N \in \mathbb{Z}^+$ and that $X_i$ has finite MGF $\forall i = 1, \ldots, N$. Define $Z = \min\{X_1, X_2, \ldots, X_N\}$. Then, the random variable, $Z$ has a finite MGF.*

*Proof.* See Appendix A. □

**Proposition 1.** *If Assumption 1 is satisfied, then the random variable, $r(a_j, \psi_\omega)$, has a finite MGF.*

*Proof.* See Appendix B. □

**Proposition 2.** *Suppose that Assumption 1 is satisfied. Then the following two properties hold for Problem (29):*

a. *for every $a_j \in A_j$, $r(a_j, \psi_\omega)$ is finite for almost every $\psi_\omega \in \Psi$; and*
b. *the function $g(a_j)$ is well defined and finite-valued for all $a_j \in A_j$.*

*Proof.* See Appendix C. □

Proposition 2 implies that both $g(a_j)$ and $g^M(a_j)$ are convex and continuous on $A_j$.

**Proposition 3.** *The objective function of SAA problem (31), $g^M(a_j)$, uniformly converges to the objective function of original problem (29), $g(a_j)$, with probability 1 (w.p.1) on $A_j$, as $M \to +\infty$.*

*Proof.* See Appendix D. □

Using the results of Propositions 2 and 3, we can appeal to the following theorem shown by Shapiro et al. (2014), which gives the convergence of an SAA. We only state this result and refer interested readers to the work of Shapiro et al. (2014) for the proof and further details.

**Theorem 1.** *Suppose that the following four properties hold:*

a. *$A^* \neq \varnothing$;*
b. *$g(a_j)$ is finite-valued and continuous on $A_j$;*
c. *$g^{m_\kappa}(a_j)$ converges to $g(a_j)$ w.p.1, as $m_\kappa \to +\infty$; and*
d. *$\hat{A}^{m_\kappa} \neq \varnothing$ w.p.1 for $m_\kappa$ sufficiently large.*

*Then, $g^{m_\kappa} \to g^*$ and $\mathbb{D}(\hat{A}^{m_\kappa}, A^*) \to 0$ w.p.1 as $m_\kappa \to +\infty$, where:*

$$\mathbb{D}(\hat{A}^{m_\kappa}, A^*) := \max_{a_j \in \hat{A}^{m_\kappa}} \operatorname{dist}(a_j, A^*).$$

*Proof.* See the work of Shapiro et al. (2014). □

Proposition 2 implies Property b. We get Property c from Proposition 3. Properties a and d are satisfied because of feasibility of the first stage and the relatively complete recourse property, which comes from Constraint (10).

### *3.6. Asymptotic Validity and Finite Termination*

The two other important questions about Algorithm 1 are whether it provides an asymptotically valid confidence interval on the optimality gap and whether the algorithm terminates, by satisfying termination criterion $\Upsilon$, in a finite number of iterations. We answer the two questions by relying on the results of Bayraksan and Morton (2011).

To answer these questions, we first show the following proposition.

**Proposition 4.** *If Assumption 1 is satisfied, $r(a_j, \psi_\omega)$ is Lipschitz continuous on $A_j$ w.p.1.*

*Proof.* See Appendix E □

We can now use Proposition 4 to appeal to the following theorem proven by Bayraksan and Morton (2011), which gives the asymptotic validity of the confidence interval and finite termination of the SAA algorithm. We only state this theorem and refer interested readers to the work of Bayraksan and Morton (2011) for further details and the proof.

**Theorem 2.** *Suppose that the following five properties hold:*

a. $g^{m_\kappa} \to g^*$ *and* $\mathbb{D}(\hat{A}^{m_\kappa}, A^*) \to 0$ *w.p.1 as* $m_\kappa \to +\infty$*;*
b. $G_{l_\kappa}(a_j) \geq D_{l_\kappa}(a_j)$*, w.p.1 for all* $a_j \in A_j$ *and* $l_\kappa \geq 1$*, where:*

$$G_{l_\kappa}(a_j) = g^{l_\kappa}(a_j) - g^{l_\kappa}(a_j^{l_\kappa *});$$

*and:*

$$D_{l_\kappa}(a_j) = g^{l_\kappa}(a_j) - g^{l_\kappa}(a_j^*);$$

*where* $g^{l_\kappa}(\cdot)$ *is defined by (31) with the parameter* $m_\kappa$ *on the right-hand side replaced with* $l_\kappa$*,* $a_j^* \in A^*$*, and* $a_j^{l_\kappa *} \in \hat{A}^{l_\kappa}$*, where:*

$$\hat{A}^{l_\kappa} = \left\{ a_j \in A_j \,\middle|\, g^{l_\kappa}(a_j) = \min_{a_j \in A_j} g^{l_\kappa}(a_j) \right\};$$

c. $\liminf_{l_\kappa \to \infty} s_{l_\kappa}^2(a_j) \geq \sigma^2(a_j)$*, w.p.1 for all* $a_j \in A_j$*;*
d. $\sqrt{l_\kappa}(D_{l_\kappa}(a_j) - \mu(a_j)) \xrightarrow{\mathcal{P}} N(0, \sigma^2(a_j))$ *as* $l_\kappa \to +\infty$ *for all* $a_j \in A_j$*, where* $\xrightarrow{\mathcal{P}}$ *means convergence in probability; and*
e. $r(a_j, \psi_\omega)$ *is Lipschitz continuous on* $A_j$*.*

*If the sample sizes used in Step 4 of Algorithm 1 satisfy (39) and the algorithm terminates by satisfying (38), then for any* $\epsilon > \epsilon' > 0$*,* $q > 0$*, and* $\alpha \in (0, 1)$ *we have that:*

$$\lim_{h \to h'^+} \inf \text{Prob}\left\{ \mu(a_j^{m_\Gamma *}) \leq h \cdot \bar{s}(a_j^{m_\Gamma *}) + \epsilon \right\} \geq 1 - \alpha;$$

*where* $a_j^{m_\Gamma *}$ *is the final solution found when Algorithm 1 terminates. Moreover, for any* $h > h' > 0$ *we have that:*

$$\text{Prob}\{\Gamma < +\infty\} = 1.$$

*Proof.* See the work of Bayraksan and Morton (2011) □

Our original and SAA problems satisfy the requirements of Theorem 2. Theorem 1 implies Property a. We get Property b from the fact that $g^{l_\kappa}(a_j^{l_\kappa *}) \leq g^{l_\kappa}(a_j^*)$. Bayraksan and Morton (2006) show that Property c holds if $r(a_j, \psi_\omega)$ is continuous with respect to $a_j \in A_j$ w.p.1, $\mathbb{E}\left[\sup_{a_j \in A_j} r^2(a_j, \psi_\omega)\right] < +\infty$, and $A_j$ is non-empty and compact. Property d is satisfied because of the central limit theorem for i.i.d. random variables. Finally, Proposition 4 gives Property e.

## 4. Case Study

The station-control model and solution technique introduced in Sections 2 and 3 are demonstrated using a case study. The case study is used to analyze the optimal scheduling of EV-charging loads and the resulting cost of operating the charging station. These cost calculations can be used to estimate the impact of building a public EV-charging station from energy- and infrastructure-cost perspectives. We also contrast the charging profiles and resulting cost given by our proposed model to three simple heuristic charging techniques. This is done to demonstrate the benefits of the proposed model in scheduling flexible EV-charging loads more intelligently than heuristics do.

The case study is based on the Central-Ohio region. It assumes that a public EV-charging station is built in the parking area of a major retail shopping center in northeastern Columbus, Ohio. The shopping center

is connected to the electricity-distribution system through an $\bar{R} = 500$ kVA transformer. This transformer, which is shared by the buildings in the retail shopping center, is also used by the EV-charging station. Thus, the transformer must serve the total EV and non-EV loads. Station operations are modeled over a representative year, using electricity-price, weather, and vehicle-usage data for the year 2013.

A number of the case study parameters (*e.g.*, the non-EV load, electricity prices, and transformer characteristics) are fixed. We examine the effects of other parameters through a fractional factorial experiment. Specifically, we examine the effects of the EV charger power capacity, whether distributed PV and BESS are installed, the EV penetration level, and the charging window through this experimental design.

We detail the datasets used and how these data are processed in constructing our case study in Sections 4.1–4.7. Section 4.8 describes our fractional factorial experimental design.

### *4.1. Electric Vehicle Usage*

EV-usage data, which are implicitly needed to determine EV arrival times and the charging demands of EVs upon their arrivals, are modeled using vehicle-driving data provided by the Mid-Ohio Regional Planning Commission (MORPC). More specifically, our work relies on two MORPC datasets: (1) tour-record data specifying the use of the approximately 1.1 million light-duty vehicles in the Central-Ohio region and (2) geographic information system data for the region, which include average vehicle-speed data for all of the road segments in the road network.

The tour records provide modeled data on the use of the 1.1 million light-duty vehicles in Central Ohio during a typical day. The data are generated using the multi-step tour-based approach discussed by Sener et al. (2009). Each tour is associated with a specific vehicle in the modeled dataset and information on subtours (*e.g.*, stopping at a retail shopping location *en route* while commuting from work to home) are included as well. The dataset also provides the starting and ending times and locations of each tour and subtour.

The MORPC data are used to simulate EV-usage patterns by following a four-step process. The first step is to determine what subset of the 1.1 million light-duty vehicles in the MORPC dataset are EVs by bootstrapping from the tour-record data. This is done by assuming an EV penetration level (as discussed in Section 4.8, we consider cases in which the EV-penetration level is 3% and 8% of the light-duty vehicle fleet of Central Ohio) and randomly selecting a corresponding number of vehicles in the tour-record data to be EVs.

The second step is to determine the path taken by each randomly selected EV as it completes each driving trip during the day. This is done by assuming that each EV owner takes the shortest-time path on each vehicle trip. Using this assumption and the road-network and average-vehicle-speed data provided by MORPC, the EV routes are determined by solving a shortest-time-path problem.

Once the vehicle paths are determined, the third step is to determine the SOC of each EV battery as it travels along its path. This is done using an assumed battery capacity of 24 kWh and a driving efficiency of 3.73 kWh/km. These values correspond to reported characteristics of a Nissan Leaf.

The fourth step is to determine which EVs use the modeled charging station. In doing so, we make two additional assumptions. The first, which follows the work of Wu and Sioshansi (2017), is that an EV driver only uses the charging station if the vehicle comes within 1.6 km (1.0 mile) of the charging station while traveling along the intended shortest path from origin to destination. The second is that an EV driver will only use the charging station if the EV battery's SOC is below some set threshold value, which we take to be 50%. This threshold value is meant to capture the perceived inconvenience of using a public charging station. An EV driver only uses one if the SOC of the EV battery is sufficiently low.

The arrival time of an EV that does use the charging station is determined based on its departure time to begin the tour that brings it within the 1.6 km radius of the station (which is reported in the tour-record data) and the driving time to arrive to the station (which is determined from the shortest-time-path problem). Its charging demand is determined based on its modeled battery SOC upon arrival at the station (assuming that the EV driver wishes its battery fully recharged). We further assume that 80% of EVs are flexible, in the sense that the charging station can schedule their charging within a $W$-minute window of time. The others are assumed to be inflexible and begin charging immediately at the $\bar{H}$ kW rated charger

capacity upon arrival to the station. The loads of such EVs are modeled by including them in the $L_j$ and $L_{t,\omega}$ state parameters. EVs are randomly assigned to be either flexible or inflexible.

Our assumptions of a fixed deviation radius (*i.e.*, that EV drivers only use a charging station if the vehicle comes within a 1.6 km radius of the charging station), is consistent with other works in the literature. Kuby et al. (2013) investigate refueling behavior of early alternative-fuel vehicle adopters. They find that the median refueling-deviation tolerance is between 0.8 miles and 1.3 miles. Our assumption of an EV driver only using the charging station if the battery SOC is below a certain threshold also follows other works in the literature. The work of Kuby et al. (2013) finds that 83.4% of alternative-fuel vehicle owners refuel their vehicles when the fuel tank is at less than 3/8 capacity. Nevertheless, our assumptions may be optimistic in modeling the charging demands EVs. Wang et al. (2011); He et al. (2013, 2016) note that in practice some EV owners may not use a public charging station while *en route* from origin to destination. They surmise, rather, that charging demands may be more concentrated among EVs that have the location of the charging station as their final destination.

Numerical simulations show that the temporal distribution of the number of vehicles that come within the 1.6 km capture radius of the charging station is bimodal. 18.6% of the vehicles that come within the capture radius in a typical day arrive between 7:00 am and 9:00 am and another 19.0% arrive between 4:00 pm and 7:00 pm, which are typical commuting times. However, very few of the EVs that come within the capture radius during the morning commute have a sufficiently low SOC to use the charging station. Less than 0.5% of the EVs that come within the capture radius between 7:00 am and 9:00 am have a battery SOC below the 50% threshold, meaning that the overwhelming majority of them would not use the charging station in the morning. This is because we assume that each EV begins each day with a fully charged battery (from overnight at-home vehicle recharging) and the relatively short cumulative driving distance that each EV has gone in the morning. Conversely, 5% of EVs that come within the capture radius between 4:00 pm and 7:00 pm have a battery SOC below the 50% threshold, meaning greater use of the charging station during the evening commute. Averaging across all of the hours, about 3% of EVs that come within the capture radius during the course of a typical day have a battery SOC below the 50% threshold. With an EV penetration level of 3% of the total light-duty vehicle fleet in Central Ohio, the charging station has 17 expected EV arrivals per day with an SOC threshold of 50%. This number increases to 45 expected daily EV arrivals with an EV penetration level of 8%.

### *4.2. Non-Electric Vehicle Load*

We model the non-EV load using data from the year 2013 provided by American Electric Power Ohio (AEP Ohio), the distribution utility company that operates in Central Ohio. The data consist of anonymized load profiles on a number of 500 kVA commercial transformers, recorded at a 15-minute time resolution. We fit an order-16 autoregressive model (*i.e.*, an AR(16) model) to generate forecasts of non-EV load for the scenarios used in the station-control model.

### *4.3. Photovoltaic Generation*

We model the real-time output of the distributed PV generator using historical weather data from the year 2013 for the city of Columbus. These weather data are input to version 5 of the PVWatts model, the use of which is described by Dobos (2014). PVWatts uses weather data to simulate the output of a hypothetical PV generator. We obtain historical solar-insolation data from the National Solar Radiation Database (NSRDB). As discussed by Sengupta et al. (2014b,a), the NSRDB models ground-level solar insolation using satellite-image data. Other weather data needed by PVWatts (*i.e.*, wind speed and temperature) are obtained from the National Oceanic and Atmospheric Administration. We run PVWatts with a one-minute temporal resolution, to obtain simulated one-minute PV-output data.

We fit an AR(6) model to the PV-output data simulated by the PVWatts model. This model is used to generate forecasts of PV availability for the scenarios used in the station-control model. The reason for using an AR(6) is that one-minute PV output is relatively unpredictable compared to forecasting PV output at longer time intervals (*e.g.*, hourly-average PV output). This is because minor weather events, such as a small patch of clouds, can drastically affect the one-minute output of a single PV panel. Conversely, a small

patch of clouds would have a relatively muted effect on the hourly-average output of the same PV panel. Our forecasting technique assumes that solar output over a longer (*e.g.*, hour-long) horizon is essentially stationary. The AR(6) model is used to generate sample paths of possible PV output at one-minute intervals, which tend to exhibit greater variability and uncertainty.

Figure 1 shows modeled PV availability data from a 200 kW panel on 5 December, 2013. The solid blue curve shows modeled actual PV output available from the between 14:54 and 15:51. These data are obtained from the PVWatts model, and are taken as actual available PV output in our simulation. The green line with dots represents one sample path of possible PV output, forecasted as of 15:11, over the remaining 40 minutes depicted in the figure. This curve shows considerable variability, as expected of a model generating forecasts at a one-minute interval. The dashed red line shows the sample-average PV output, which is obtained by generating multiple sample paths of the forecasts.

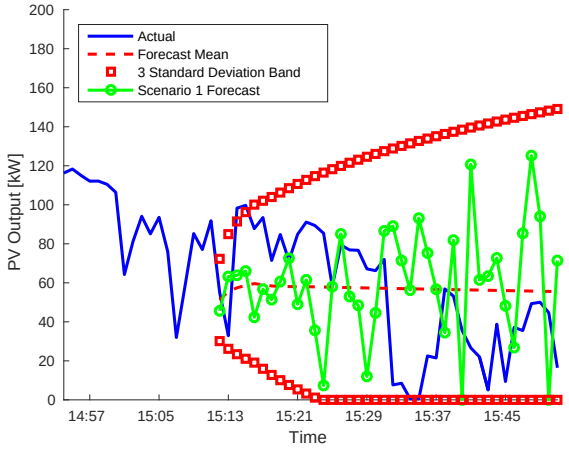


Figure 1: Modeled PV Availability From a 200 kW Panel on 5 December, 2013: Actual and Forecast Mean, Three-Standard Deviation Band, and Scenario-1 Forecast as of 15:11

As expected, the sample-average PV output exhibits considerably less variability than an individual sample path. Moreover, the sample average is roughly stationary. The pair of red curves labeled with squares shows a three-standard deviation band around the sample-average mean. Again, the wide (and growing) range of this band shows that individual sample paths can have significant variability and that this variability grows as we generate forecasts further into the future. The band is truncated below at zero, because it is physically meaningless to have a PV panel produce a negative amount of power.

### *4.4. Electricity Price*

Real-time electricity prices are forecasted using an AR(8) model that is fit to hourly historical real-time prices from 2013. Specifically, we use real-time prices for the AEP zone of the PJM Interconnection market, which covers the AEP Ohio service territory. Our model assumes that the real-time price is constant over each one-hour period, which is consistent with wholesale-pricing practice in PJM. Thus, unlike the AR model that is used for PV forecasting, which uses a one-minute timestep, this AR(8) model uses an hourly timestep. This is because the types of variability in PV output that we seek to capture occur on one-minute timescales. Conversely, the important variability in energy prices occur on hourly timescales. As is common practice in wholesale electricity markets, our model allows for negative energy prices.

### *4.5. Battery Energy Storage System Characteristics*

We assume that the BESS has upper and lower bounds on its SOC of $\bar{S}^{E,+} = 4200$ kW-min (70 kWh) and $\bar{S}^{E,-} = 1200$ kWh (20 kWh), respectively, and a power capacity of $\bar{S}^{P} = 100$ kW. We also assume charging and discharging efficiencies of $\mu^c = \mu^d = 0.99$. These values are typical for a lithium-ion BESS, as reported by Xi and Sioshansi (2016).

### *4.6. Transformer Characteristics*

Our case study assumes that the charging station is connected to the power system through a 500 kVA transformer, which it shares with the retail shopping center where the station is located. Our model allows the transformer to operate above its 500 kVA design capacity. However, doing so places additional strain on the transformer, causing it to age and deteriorate more rapidly.

We capture this accelerated aging using the model introduced by Gong et al. (2011). This model simulates the effects of operating a transformer above its design capacity on the temperature of the windings in the transformer, which is the component that is typically prone to failure from such overloading. More specifically, we use the model to estimate the service life of the transformer if it is operated at its design capacity of 500 kVA. We then determine what effect operating the transformer above the 500 kVA design capacity has on reducing its service life. This reduction in service life is combined with an assumed \$10000 replacement cost for a transformer, to derive the following piecewise-linear convex penalty function:

$$R^C(v_j) = \begin{cases} 1.16v_t, & \text{if } v_t \in [0, 0.4\bar{R}); \\ 42.65(v_t - 0.4\bar{R}) + 232.70, & \text{if } v_t \in [0.4\bar{R}, 0.6\bar{R}); \\ 764.62(v_t - 0.6\bar{R}) + 4497.35, & \text{if } v_t \in [0.6\bar{R}, 0.8\bar{R}); \\ 12309.73(v_t - 0.8\bar{R}) + 80959.50, & \text{if } v_t \in [0.8\bar{R}, +\infty); \end{cases}$$

for operating the transformer above its design capacity. Although we model $R^C(\cdot)$ as being piecewise-linear, it is a convex function. Thus, binary variables are not needed and this cost can be modeled using continuous variables while maintaining a linear objective function in our model.

### *4.7. Temporal Resolution*

Our model uses a one-minute temporal granularity in scheduling EV charging and making BESS-charging and -discharging decisions. The model has a $T = 60$ minute optimization horizon. This is a reasonable model horizon, because each EV can be fully recharged within at most 30 minutes, based on the assumed capacity of the EV batteries and the power capacity of the EV chargers (*i.e.*, 30 minutes is how long it would take for a fully depleted EV battery to be fully recharged). As a result, the primary control decision, which is how much EV-charging load to schedule in the current minute as opposed to deferring for later, can only be delayed by at most 30 minutes into the future. As such, the state of the charging station more than 60 minutes in the future is expected to have a relatively insignificant effect on the current-minute scheduling decision.

### *4.8. Fractional Factorial Experimental Design*

The operations of a public EV charging station depend on a number of factors that are either uncertain or need to be determined by the station designer. We examine the impacts of five such factors—$\bar{H}$ (the power capacity of the EV charger), whether distributed PV or BESS are installed in the charging station, the EV penetration level (as a percentage of the light-duty vehicle fleet in Central Ohio), and $W$ (the charging window for flexible EVs)—through a fractional factorial experiment. We assume that each of these five factors have two possible values. Table 1 lists the eight cases, with different combinations of factors, examined. Note that a full factorial experiment would require the evaluation of $2^5 = 32$ cases. We opt to conduct the fractional design summarized in Table 1, which assumes only first- and second-order interactions amongst the factors. We conduct this fractional experiment because a full factorial experiment would be computationally expensive.

We can examine the effects of different factors by averaging the cases corresponding to that factor. For instance, we can estimate the operating cost with a BESS installed in the charging station by averaging the operating costs given in Cases 2, 4, 6, and 8. We can then contrast this with the operating cost without a BESS installed, which is given by averaging across Cases 1, 3, 5, and 7. This averaging allows us to determine the impacts on operating cost of having a BESS installed, without other factors confounding the results.

Table 1: Fractional Factorial Experimental Design

| Case | $\bar{H}$ [kW] | PV | BESS | EV Penetration | $W$ [min] |
|---|---|---|---|---|---|
| 1 | 120 | no PV | no BESS | 3% | 40 |
| 2 | 50 | no PV | BESS | 3% | 30 |
| 3 | 50 | 200 kW | no BESS | 3% | 40 |
| 4 | 120 | 200 kW | BESS | 3% | 30 |
| 5 | 120 | no PV | no BESS | 8% | 30 |
| 6 | 50 | no PV | BESS | 8% | 40 |
| 7 | 50 | 200 kW | no BESS | 8% | 30 |
| 8 | 120 | 200 kW | BESS | 8% | 40 |

## 5. Case-Study Results

We use the case study outlined in Section 4 to analyze the EV-charging station in two ways. First, in Section 5.1 we demonstrate the use of the station-control model over a one-year period assuming a fixed station design that consists of a 70 kWh/100 kW BESS, a 200 kW distributed PV system, $\bar{H} = 120$ kW EV chargers, an EV-penetration level of 8%, and a $W = 40$ minute charging window for flexible EVs. We also compare the charging profiles given by our station-control model to three simple heuristics, demonstrating the benefits of our proposed model. This analysis is done using the fractional factorial experiment, which is outlined in Section 4.8, to examine cases with EV penetration levels of 3% and 8% and with 30- and 40-minute charging windows. Next, in Section 5.2 we examine the sensitivity of charging-station operations to having distributed BESS and PV solar or not and the power capacity of the EV chargers. This analysis is also conducted using the fractional factorial experiment.

### *5.1. Station-Control Model Results*

We first examine the charging profiles and resulting transformer-load profiles given by the station-control model under a fixed station-design. This analysis assumes that the charging station consists of a 70 kWh/100 kW BESS, 200 kW distributed PV system, and $\bar{H} = 120$ kW EV chargers. We further assume an EV-penetration level of 8% and a $W = 40$ minute charging window for flexible EVs. Figure 2 shows the total load on the transformer over a 2.5-hour-long period of time if EV charging loads are scheduled using the proposed station-control model. It also shows the transformer load if EV charging is instead scheduled using a simple first-come, first-served (FCFS) heuristic. This FCFS heuristic assumes that each EV immediately begins charging at the $\bar{H} = 120$ kW charger capacity until it is fully recharged (*i.e.*, it assumes that the flexibility in scheduling EV-charging loads is not used).

Figure 2a shows that under a FCFS heuristic, the transformer is operated above its 500 kVA design capacity whereas the station-control model schedules EV charging loads to keep the load below this level. Over the course of the entire day shown in Figure 2, the FCFS heuristic results in the transformer operating above the 500 kVA design capacity for 54 minutes, as opposed to never operating above this capacity with the proposed station-control model.

Figure 2b shows that the distributed PV and BESS play limited roles in helping to manage EV-charging loads. As discussed in Section 4.1, most of the EV arrivals to the charging station occur during the evening commute home, when PV output is beginning to taper off as the sun is setting. As a result, the primary benefit of the distributed PV system is to help reduce the use of grid-purchased energy to serve the non-EV load midday.

Moreover, EV loads are mostly managed by shifting them within the $W$-minute charging window. The BESS is only used in a limited fashion when there is insufficient flexibility to keep the transformer load below its 500 kVA capacity. The BESS is only discharged in 17 minutes of the entire day shown in Figure 2. During these 17 minutes it is discharged, on average, at 70 kW, which is far short of its $\bar{S}^P = 100$ kW capacity. The reason for this is that shifting EV-charging loads is a cost-free means of keeping the transformer load

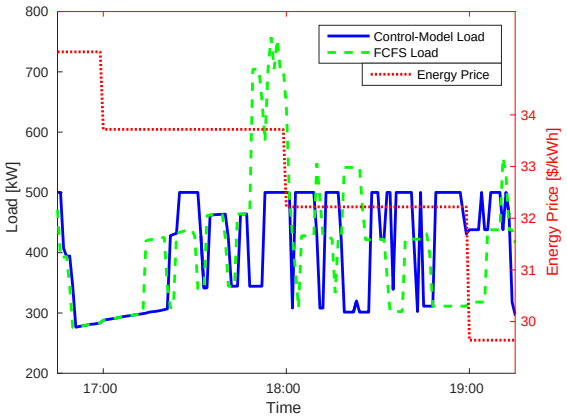


(a) Transformer-Load and Energy-Price Profiles

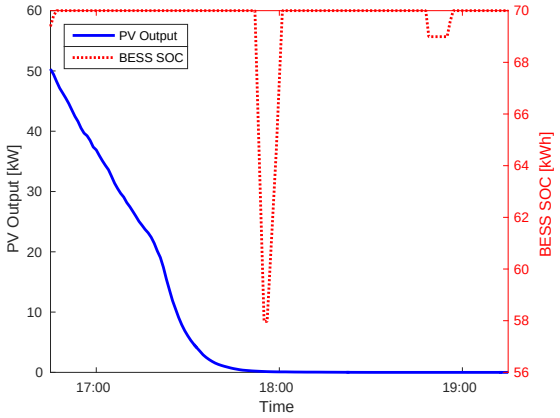


(b) Photovoltaic Generation and Battery Energy Storage System State of Charge

Figure 2: Transformer-Load Profile From Station-Control Model and Using First-Come, First-Served Heuristic

below 500 kVA. Using the BESS imposes a small cost of about 2% (relative to the wholesale energy price), due to the loss of energy when charging and discharging the BESS. As a result, the model prefers shifting EV-charging loads and only uses the BESS when there is insufficient flexibility to keep the load below 500 kVA. Otherwise, if there is no BESS capacity available (or in cases without a BESS installed) and there is insufficient flexibility availability to shift EV-charging loads, the model is forced to load the transformer above its 500 kVA capacity. Instances in which this occurs are illustrated in Sections 5.1.2 and 5.2.

The station-control model and the solution method proposed in Section 3 are implemented using CPLEX version 12.6.1. When run on a computer with a 3.0 GHz Intel Pentium G3220 Processor and 16 GB of memory, each instance of the one-minute station-control models takes an average of 39.44 seconds of CPU time to run.

*5.1.1. Effect of First-Come, First-Served Policy on Transformer Aging*

Figure 2 shows that one of the most severe impacts of relying on a simple heuristic, such as FCFS, is that the transformer can be easily overloaded, especially in the afternoon when many EVs simultaneously arrive to the station. Figure 3 shows the effects on the expected operational life of the 500 kVA transformer of relying on a FCFS heuristic. It shows the expected lifetime of the transformer under different EV penetration levels and with different threshold SOC levels at which EV owners use the public charging station.

We estimate the expected lifetime of the transformer by randomly simulating 1000 replications of EV-usage, PV generation, and non-EV load data over a one-year period. Each of the 1000 resulting load profiles

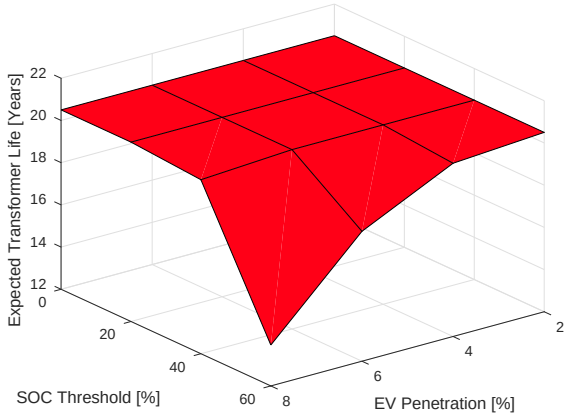


Figure 3: Expected Operational Life of 500 kVA Transformer Using a First-Come, First-Served Heuristic With Different Electric Vehicle Penetration Levels and Charging Thresholds

are then simulated in the transformer aging model of Gong et al. (2011), by assuming that the load profiles repeat year after year, to determine the lifetime of the transformer under that load profile. Thus, we do not account for load growth over the lifetime of the transformer, which would accelerate transformer aging relative to what is reported in Figure 3.

Distribution transformers normally have a planned operational life of 20.5 years. The figure shows that in many instances, the FCFS heuristic does not reduce the expected life of the transformer below this level. However, in cases in which the SOC threshold is below 40% and the EV-penetration level is above 4%, the expected life of the transformer can be reduced, on average, by up to 32% relative to the 20.5-year design life. Moreover, some of the random replications used to simulate transformer aging result in load profiles with extreme peaks that reduce the expected life of the transformer to 0.057 years (21 days). Although the likelihood of such a load profile is small, this result nevertheless points out the importance of managing EV-charging loads from the perspective of reducing the cost of having to replace distribution infrastructure. Without some form of charging management, which would yield FCFS EV-charging profiles, there would be considerable risk of added costs associated with upgrading electricity-distribution infrastructure.

*5.1.2. Comparison of Station-Control Model and Heuristic Scheduling Techniques*

FCFS is a relatively simple heuristic in which the flexibility of EV charging is not exploited in any way, because EV-charging loads are served immediately without any scheduling. Thus, we examine two other heuristic charging-control techniques.

The first, which we refer to as Constrained FCFS, has the same basic premise as the FCFS heuristic. When an EV arrives to the station, it immediately begins charging at the $\bar{H}$ kW capacity of the charger, so long as doing so does not overload the transformer. If charging the newly arrived EV would overload the transformer, the newly arrived EV instead queues and waits for one of the EVs that is currently charging to finish charging, at which point the newly arrived EV begins charging. If another EV arrives while an earlier arrival is queuing, this newly arrived EV also queues. The Constrained FCFS heuristic is guaranteed not to overload the transformer, because each EV only charges so long as there is transformer capacity available. However, the Constrained FCFS heuristic may result in an EV not being able to fully recharge within the $W$-minute window of time.

We refer to the other heuristic as Uniform Charging. Upon arrival to the charging station, each EV charges at $(F/W)$ kW, where $F$ is the total charging demand of the EV upon arrival to the station measured in kW-min. Thus, the Uniform Charging heuristic has each EV spread its charging demand uniformly over the $W$-minute charging window. By design, the Uniform Charging heuristic is guaranteed to fully recharge each EV. However, it is possible that the transformer can be overloaded if too many EVs arrive within a short span of time.

Figure 4 shows the load-duration curves of the 1000 hours of the year with the highest load on the transformer when EV charging is scheduled using our proposed station-control model and the three heuristics. The four figures show the load-duration curve for four different settings, in which the charging window is either 30 or 40 minutes and the EV penetration level is 3% or 8% of the light-duty vehicle fleet of Central Ohio. The figures are generated by conducting the fractional factorial design discussed in Section 4.8, and each figure shows the corresponding average load-duration curve. For instance, Figure 4a, which corresponds to having a 3% EV penetration, shows the average load-duration curve among Cases 1–4 in Table 1.

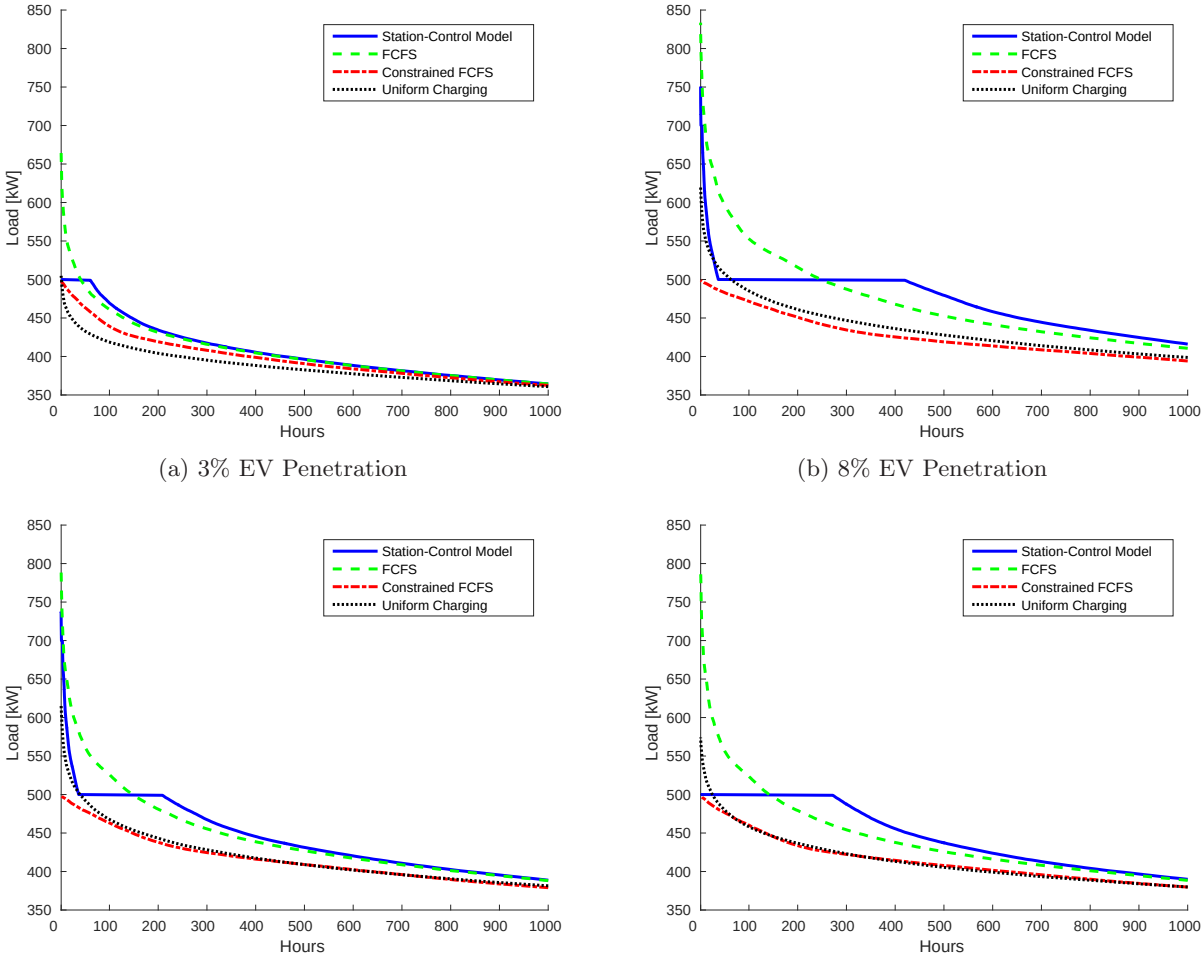


(a) 3% EV Penetration

(b) 8% EV Penetration

(c) $W = 30$ Minutes

(d) $W = 40$ Minutes

Figure 4: Load-Duration Curve of 1000 Hours of the Year With Highest Transformer Loads Under Station-Control Model and Three Heuristics

As expected, the figure shows that the proposed model significantly reduces the number of hours in which the transformer is operated above its 500 kVA capacity. The only heuristic that outperforms the station-control model on this metric is the Constrained FCFS heuristic, which is designed to keep the transformer load below 500 kVA at all times. Tables 2 and 3 summarize the performance of the station-control model and the three heuristics on two key metrics.

Table 2 lists the average (using the fractional factorial experimental design) number of hours in which the transformer is operated above its 500 kVA capacity in the different cases examined and the peak transformer load. Values for the Constrained FCFS heuristic are not listed, because, by definition, this heuristic never overloads the transformer. The table shows that the station-control model outperforms the heuristics in

Table 2: Average Peak Load and Number of Hours Over the Year That the Transformer is Overloaded With Station-Control Model and First-Come, First-Served and Uniform Charging Heuristics

| | | Case | | | |
|---|---|---|---|---|---|
| | | 3% EV Penetration | 8% EV Penetration | $W = 30$ Minutes | $W = 40$ Minutes |
| Overload Duration [hours] | Control Model | 0.2 | 36.8 | 36.4 | 0.6 |
| | FCFS | 40.1 | 244.9 | 145.5 | 139.5 |
| | Uniform Charging | 1.4 | 61.2 | 38.4 | 24.1 |
| Peak Load [kW] | Control Model | 542 | 916 | 725 | 734 |
| | FCFS | 869 | 1325 | 1325 | 1050 |
| | Uniform Charging | 591 | 727 | 727 | 680 |

Table 3: Average Unserved Electric Vehicle-Charging Load Over the Year With Constrained First-Come, First-Served Heuristic

| | Case | | | |
|---|---|---|---|---|
| | 3% EV Penetration | 8% EV Penetration | $W = 30$ Minutes | $W = 40$ Minutes |
| Unserved EVs | 678 | 4935 | 3050 | 2562 |
| Unserved EV Load [kWh] | 5663 | 47664 | 28667 | 24661 |

terms of the number of hours in which the transformer is overloaded. However, in some of the cases the station-control model puts a higher peak load on the transformer. This is because there is an inherent tradeoff when there are many EVs needing to have their charging loads satisfied. The Uniform Charging heuristic spreads these loads more evenly, which can result in a lower peak load but the transformer being overloaded in more hours. The station-control model, conversely, opts to concentrate these loads in a fewer number of hours, which can give a higher peak but fewer overloaded hours.

Unlike the other heuristics and station-control model, the Constrained FCFS heuristic can result in EVs not being fully recharged. Table 3 summarizes the average (using the fractional factorial experiment) number of EVs that are not fully recharged over the course of the year and the total unserved EV charging load if the Constrained FCFS heuristic is employed. With our assumed EV efficiency of 3.73 kWh/km, the Constrained FCFS results in the equivalent of between 1518 km and 12779 km of EV charging demand not being satisfied over the course of the year.

Table 4 provides summary statistics of the resulting average daily operation cost of the charging station using our proposed station-control model and the three heuristics. The summary statistics reported are the mean, median, third quartile, and maximum (among the 450 replications of EV-usage, PV generation, and non-EV load data over the one-year period simulated). The proposed control model and the two 'more intelligent' heuristics (Constrained FCFS and Uniform Charging) all outperform FCFS in terms of all four summary statistics. Moreover, our proposal charging-control model outperforms the two intelligent heuristics on this cost metric as well. Although the daily operation costs reported in Table 4 for the Constrained FCFS heuristic are lower than those reported for the control model, these costs do not account for unserved EV-charging demand under the Constrained FCFS heuristic. If we assume a value of lost of load of \$3.72/kWh, which is the value reported by Kariuki and Allan (1996), unserved EV-charging loads increase the daily operation cost of the Constrained FCFS heuristic by an average of at least \$251.34. This makes the control strategies given by this heuristic twice as costly as those provided by our proposed charging-control model.

### *5.2. Parameter Sensitivity Analysis*

We now examine the effects of changing a number of the model parameters in our case study on the performance of our station-control model, using the fractional factorial experimental design discussed in

Table 4: Average Daily Operation Cost [$] of Charging Station with Station-Control Model and First-Come, First-Served; Constrained First-Come, First Served; and Uniform Charging Heuristics Assuming 8% Electric Vehicle Penetration and a $W = 40$ Minute Charging Window

| | Control Method | | | |
|---|---|---|---|---|
| | Control Model | FCFS | Constrained FCFS | Uniform Charging |
| Mean | 262.90 | 1080.50 | 261.00 | 266.70 |
| Median | 237.56 | 336.69 | 236.71 | 238.30 |
| Third Quartile | 282.06 | 782.72 | 281.25 | 283.26 |
| Maximum | 1151.40 | $1.97 \times 10^5$ | 1134.40 | 1253.60 |

Section 4.8. Specifically, we examine the effect of removing the BESS and distributed PV generator and the effect of reducing the power capacity of the EV chargers. This analysis is done by simulating the station-control model over a one-year period using 450 replications of EV-usage, PV generation, and non-EV load data) under the different cases listed in Table 1, and averaging the resulting costs, load profiles, and other key metrics across the cases corresponding to each parameter examined.

*5.2.1. Battery Energy Storage System*

Figure 5 shows the average load-duration curves of the 1000 hours of the year with the highest load on the transformer with and without the distributed BESS installed in the charging station. The figure shows that the BESS improves the loading on the transformer by allowing some relief of the transformer during high-load periods. The BESS reduces the average duration of time that the transformer is overloaded during the year from 36.6 hours without the BESS to 0.4 hours with the BESS. The BESS also reduces the average peak load on the transformer from 766.7 kW to 691.4 kW. This comes with an increase in the average number of hours that the transformer is operating close to its capacity, however, because the BESS must be charged to provide this relief. Without the BESS the transformer is operated at between 400 kVA and 500 kVA for an average of about 786.4 hours as opposed to 834.8 hours with the BESS.

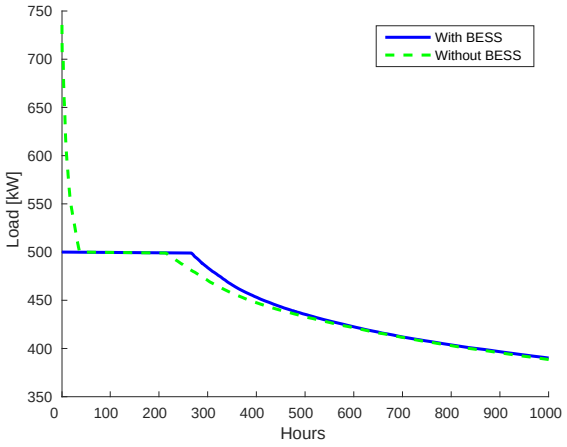


Figure 5: Average Load-Duration Curve of 1000 Hours of the Year With Highest Transformer Loads With and Without Battery Energy Storage System

The BESS also increases total average energy consumption of the distribution circuit (*i.e.*, including EV and non-EV loads) over the year by about 1 MWh. The increased load is due to energy losses when storing and discharging energy into and from the BESS. However, the BESS gives an average annual reduction in operation costs of about 72%, from $720000 without the BESS to $200000 with the BESS. These cost

savings are entirely from reduced transformer aging, which are very slightly offset by the increased energy consumption.

*5.2.2. Photovoltaic Generator*

Figure 6 shows the average load-duration curves of the 1000 hours of the year with the highest load on the transformer with and without the distributed PV generator. While the PV generator does improve the load profile, its impact is more limited compared to the BESS. This is because PV generation tends to taper off during the afternoon and evening commute hours, when most EVs arrive at the charging station. More specifically, on average about 75.3% of daily EV-charging demand arrives to the charging station after 5:00 pm. However, the PV generator only produces 0.5% of its total output after 5:00 pm.

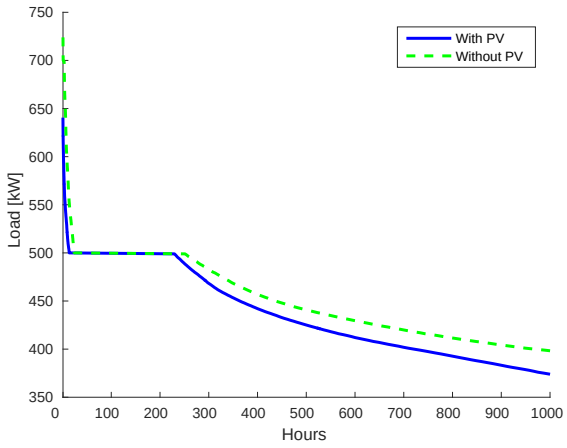


Figure 6: Average Load-Duration Curve of 1000 Hours of the Year With Highest Transformer Loads With and Without Photovoltaic System

Nevertheless, the PV generator does reduce the average load on the transformer by 12% from 316.7 kW to 279.6 kW. It has a more limited effect on the peak load, reducing it from 745.0 kW to 713.1 kW. The PV generator also reduces the average duration of time that the transformer is overloaded by 42% from 23.4 hours to 13.6 hours. However, the PV generator has a greater load-reduction effect during relatively low-load periods than during peak-load periods. During hours that the total EV and non-EV load is between 0 kW and 500 kW, the PV generator reduces transformer loading by an average of 12.0%. On the other hand, the PV generator only gives an average of a 6.8% reduction in transformer loading during hours that the total EV and non-EV load is greater than 500 kW. There is, nevertheless, a 58% reduction in average annual station-operation costs from $650000 without the PV generator to $270000 with the PV generator.

*5.2.3. Electric Vehicle Charger Power Capacity*

Figure 7 shows the average load-duration curves of the 1000 hours of the year with the highest load on the transformer with 120 kW and 50 kW EV chargers. 50 kW chargers reduce transformer loading by simply reducing the maximum amount of power that the EVs can draw. In net, the duration of time that the transformer is overloaded during the year is reduced on average by 43% from 23.6 hours to 13.4 hours with 50 kW chargers. There is also a 15% average reduction in the peak load from 786.4 kW to 671.7 kW.

## 6. Conclusion

This paper presents a model to schedule EV charging. Our proposed use of the model is to manage EV-charging loads at a public station that has fast chargers installed. Fast chargers can result in extreme peaks in the load on a radial distribution line serving the station. One way to accommodate such a load profile is to increase the capacity of the distribution infrastructure, including distributed transformers. This is likely

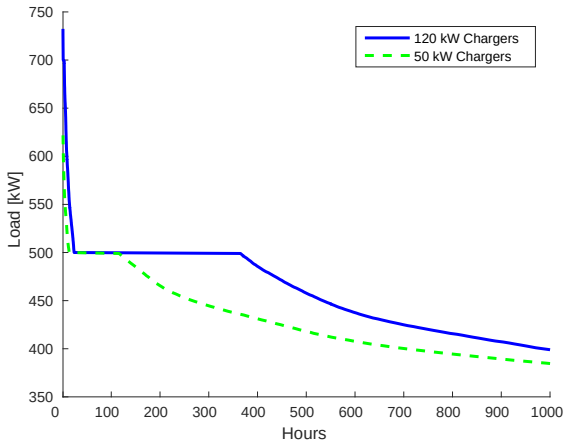


Figure 7: Average Load-Duration Curve of 1000 Hours of the Year With Highest Transformer Loads With 120 kW and 50 kW Electric Vehicle Chargers

an inefficient solution, however, because the peaks in the load profile only occur during a limited window of time when EVs are commuting home from work. Our model manages these loads by using the flexibility in recharging EVs while they are parked. Our model also allows for the use of distributed resources, such as PV and BESS, to help manage the load.

We also propose a solution technique, which employs SAA and Benders's decomposition, to efficiently solve the resulting two-stage station-control problem. We employ an SSP to estimate and control the quality of the solutions obtained from the SAA. Our numerical experiments show that when implemented on a standard computer, the proposed technique is able to give solutions that have an optimality-gap-to-standard-deviation ratio of 0.9 within an average of 39.44 seconds. This means that the model could be employed in the control system of a public charging station.

We demonstrate the use of the model using a case study based on Central Ohio. We show the benefit of the proposed model in serving EV-charging loads while minimizing the impacts of the resulting load profile on the distribution transformer. We also show the benefits of the proposed model compared to using simple heuristics, such as Constrained FCFS and Uniform Charging. Our results suggest that without a control model, such as the one that we propose, a public EV fast charging station would likely require costly transformer upgrades.

We also conduct a fractional factorial experiment to determine the impacts of distributed BESS and PV on managing charging-station loads. While these technologies have some benefits, they are relatively small compared to the benefits obtained from directly managing and scheduling EV-charging loads. Thus, our results suggest that if EVs have flexibility in having their charging loads scheduled, this flexibility provides an effective and cost-free means of reducing the distribution-impacts of EV charging. One question that our work does not address is what the optimal mix of transformer upgrades and distributed PV and BESS are to minimize the infrastructure and energy cost of operating the charging station. This is an area of future research that our model could be employed to address.

## Acknowledgments

The authors thank Armin Sorooshian, the editors, and one anonymous referee for helpful discussions and suggestions. The material in this paper is based upon work financially supported by the United States Department of Energy under Award Number DE-PI0000012 and by the National Science Foundation through Grant Number 1029337. This work was also supported by an allocation of computing time from the Ohio Supercomputer Center. Any opinions and conclusions expressed in this paper are solely those of the authors.

## Appendix A. Proof of Lemma 1

*Proof.* Because each $X_i$ has a finite MGF, this means that if we define:

$$M_i(\gamma) = \mathbb{E}\left[e^{\gamma X_i}\right] = \int_0^{+\infty} \text{Prob}\left\{e^{\gamma X_i} \geq y\right\} dy; \forall i = 1, \ldots, N;$$

then there exist values $\gamma_0^i > 0, \forall i = 1, \ldots, N$ such that:

$$M_i(\gamma) < +\infty, \forall i = 1, \ldots, N; \gamma \in (-\gamma_0^i, \gamma_0^i).$$

Define:

$$M_Z(\gamma) = \mathbb{E}\left[e^{\gamma Z}\right] = \int_0^{+\infty} \text{Prob}\left\{e^{\gamma Z} \geq y\right\} dy.$$

It is trivial to show that $M_Z(0) = 1$. Fix a value of $\gamma_0 = \min\left\{\gamma_0^1, \ldots, \gamma_0^N\right\}$. For any $\gamma \in (0, \gamma_0)$ we have that:

$$\begin{aligned}
M_Z(\gamma) &= \int_0^{+\infty} \text{Prob}\left\{e^{\gamma Z} \geq y\right\} dy \\
&= \int_0^{+\infty} \text{Prob}\left\{e^{\gamma X_1} \geq y, \ldots, e^{\gamma X_N} \geq y\right\} dy \qquad \text{(A.1)} \\
&= \int_0^{+\infty} \prod_{i=1}^{N} \text{Prob}\left\{e^{\gamma X_i} \geq y\right\} dy \qquad \text{(A.2)} \\
&\leq \int_0^{+\infty} \text{Prob}\left\{e^{\gamma X_k} \geq y\right\} dy \qquad \text{(A.3)} \\
&= M_k(\gamma) \\
&< +\infty.
\end{aligned}$$

Equation (A.1) follows because we have that $e^{\gamma x}$ monotonically increases with respect to $x$ for $\gamma > 0$. As such:

$$\left\{e^{\gamma \min\{X_1, \ldots, X_N\}} \geq y\right\} \equiv \left\{e^{\gamma X_i} \geq y; \forall i = 1, \ldots, N\right\}.$$

Equation (A.2) then follows because of the assumed independence of the $X_i$'s. We define the $k$ in (A.3) as:

$$k \in \arg\max_i \left\{\text{Prob}\left\{e^{\gamma X_i} \geq y\right\}\right\}.$$

Inequality (A.3) follows because:

$$0 \leq \text{Prob}\left\{e^{\gamma X_i} \leq y\right\} \leq \text{Prob}\left\{e^{\gamma X_k} \leq y\right\} \leq 1; \forall i = 1, \ldots, N.$$

We next examine the case of any $\gamma \in (-\gamma_0, 0)$, which has that:

$$\begin{aligned}
M_Z(\gamma) &= \int_0^{+\infty} \text{Prob}\left\{e^{\gamma Z} \geq y\right\} dy \\
&= \int_0^{+\infty} \text{Prob}\left\{\max\{e^{\gamma X_1}, \ldots, e^{\gamma X_N}\} \geq y\right\} dy \qquad \text{(A.4)} \\
&= \int_0^{+\infty} \left(1 - \text{Prob}\left\{\max\{e^{\gamma X_1}, \ldots, e^{\gamma X_N}\} < y\right\}\right) dy \\
&= \int_0^{+\infty} \left(1 - \prod_{i=1}^{N} \text{Prob}\left\{e^{\gamma X_i} < y\right\}\right) dy \qquad \text{(A.5)} \\
&= \int_0^{+\infty} \left(1 - \prod_{i=1}^{N} \left(1 - \text{Prob}\left\{e^{\gamma X_i} \geq y\right\}\right)\right) dy \\
&\leq \sum_{j=1}^{J} \int_{\chi_j} \left(1 - \left(1 - \text{Prob}\left\{e^{\gamma X_{\nu_j}} \geq y\right\}\right)^N\right) dy \qquad \text{(A.6)} \\
&\leq \sum_{j=1}^{J} \int_{\chi_j} \left(1 - \left(1 - N \cdot \text{Prob}\left\{e^{\gamma X_{\nu_j}} \geq y\right\}\right)\right) dy \qquad \text{(A.7)} \\
&= N \cdot \sum_{j=1}^{J} \int_{\chi_j} \text{Prob}\left\{e^{\gamma X_{\nu_j}} \geq y\right\} dy \\
&= N \cdot \sum_{i=1}^{N} \int_{\mathcal{Y}_i} \text{Prob}\left\{e^{\gamma X_i} \geq y\right\} dy \\
&\leq N \cdot \sum_{i=1}^{N} \int_0^{+\infty} \text{Prob}\left\{e^{\gamma X_i} \geq y\right\} dy \\
&= N \cdot \sum_{i=1}^{N} M_i(\gamma) \\
&< +\infty.
\end{aligned}$$

Equation (A.4) holds because $e^{\gamma x}$ monotonically decreases with respect to $x$ for $\gamma < 0$ and (A.5) follows because of the independence of the $X_i$'s. The intervals, $\chi_j$, in (A.6) are defined as $\chi_j = [\delta_j^-, \delta_j^+)$ and partition the interval, $[0, +\infty)$, such that $|\mathcal{V}_j| = 1$, where:

$$\mathcal{V}_j = \arg\min_i \left\{ 1 - \text{Prob}\left\{e^{\gamma X_i} \geq y\right\} \middle| \, y \in \chi_j \right\}.$$

That is, there is a single random variable, $X_i$, which dominates all of the others in the sense that:

$$1 - \text{Prob}\left\{e^{\gamma X_i} \geq y\right\} < 1 - \text{Prob}\left\{e^{\gamma X_j} \geq y\right\};$$

for all $j \neq i$ and $y \in \chi_j$. The breakpoints of the intervals (*i.e.*, the $\delta_j^-$'s and $\delta_j^+$'s) are crossing points at which the dominant random variable changes. Thus, we have that $\bigcup_{j=1}^{J} \chi_j = [0, +\infty)$ and $\chi_j \bigcap \chi_k = \varnothing, \forall j \neq k$.

Each interval, $\chi_j$, has a corresponding index of the $X_i$'s, $\nu_j$, associated with it. We have that $\nu_j \in \mathcal{V}_j$. Thus, $X_{\nu_j}$ is the random variable that minimizes the probability, $1 - \text{Prob}\left\{e^{\gamma X_i} \geq y\right\}$, on the interval $\chi_j$. We also define $\mathcal{Y}_i = \bigcup_{\nu_j = i} \chi_{\nu_j}$. Because $|\mathcal{V}_j| = 1$, $\mathcal{Y}_i \bigcap \mathcal{Y}_k = \varnothing, \forall i \neq k$. We also note that $\mathcal{Y}_i \subset [0, +\infty)$.

Inequality (A.6) follows from these definitions of $\chi_j$ and $\nu_j$. Inequality (A.7) then follows by applying Bernoulli's inequality to (A.6). Thus, we have that the random variable, $Z$, has a finite MGF. □

## Appendix B. Proof of Proposition 1

*Proof.* We begin by rewriting (30) as:

$$r(a_j, \psi_\omega) = \min_{u_\omega \in U_\omega} \sum_{t=j+1}^{j+T} p_{t,\omega} \cdot (e^c_{t,\omega} - e^d_{t,\omega} + f_{t,\omega} + L_{t,\omega} - V_{t,\omega}) + R^C(v_{t,\omega}).$$

For notational convenience, we define:

$$\tilde{r}(u_\omega, a_j, \psi_\omega) = \sum_{t=j+1}^{j+T} p_{t,\omega} \cdot (e^c_{t,\omega} - e^d_{t,\omega} + f_{t,\omega} + L_{t,\omega} - V_{t,\omega}) + R^C(v_{t,\omega}).$$

We define the random vector:

$$\zeta = (V_{j+1,\omega}, \ldots, V_{j+T,\omega}, L_{j+1,\omega}, \ldots, L_{j+T,\omega}, N_{j+1,\omega}, \ldots, N_{j+T,\omega}, F_{j+1,\omega}, \ldots, F_{j+T,\omega}).$$

For all $a_j \in A_j$ and $\hat{u}_\omega \in U_\omega$, the conditional random variable, $\{h(\hat{u}_\omega, a_j, \psi_\omega)|\zeta\}$, has a finite MGF. This is because (10) guarantees relatively complete recourse and because of Assumption 1. Thus, we have that the conditional random variable:

$$\{r(a_j, \psi_\omega)|\zeta\} = \min_{\lambda \in \Lambda(a_j, \psi_\omega)} \left\{\tilde{r}(u^\lambda_\omega, a_j, \psi_\omega)|\zeta\right\};$$

where $\Lambda(a_j, \psi_\omega)$ is the set of extreme-points of feasible region $U_\omega$, given $a_j$ and $\psi_\omega$. Note that $|\Lambda(a_j, \psi)|$ is finite. Based on Lemma 1, the conditional random variable, $\{r(a_j, \psi_\omega)|\zeta\}$, has a finite MGF. Assumption 1 ensures that $\zeta$ is bounded. Therefore, $r(a_j, \psi_\omega)$ has a finite MGF. □

## Appendix C. Proof of Proposition 2

*Proof.* To show Property a, we note that (10) guarantees that the problem has relatively complete recourse. This guarantees the existence of a feasible second-stage solution for all $a_j \in A_j$ and for almost every $\psi_\omega \in \Psi$ (*i.e.*, the event $\{r(a_j, \psi_\omega) = +\infty\}$ has measure zero $\forall a_j \in A_j$). Moreover, because $U_\omega$ is bounded for all $\psi_\omega \in \Psi$, we have that $r(a_j, \psi_\omega) > -\infty$ for almost every $\psi_\omega \in \Psi$ and for every $a_j$.

To show Property b, we first note that it is easy to show that $r(a_j, \psi_\omega)$ is piecewise-linear convex in $a_j$ for almost every $\psi_\omega \in \Psi$. Thus, $\mathbb{E}[r(a_j, \psi_\omega)]$ is well defined. Because of Proposition 1, the first moment of $r(a_j, \psi_\omega)$ is finite. We further have that $c_j(a_j, \xi_j)$ is well defined and finite. Thus, $g(a_j)$ is well defined and finite. □

## Appendix D. Proof of Proposition 3

*Proof.* We know from Proposition 1, that the second moment of $r(a_j, \psi_\omega)$ is finite. Because $c_j(a_j, \xi_j)$ is also finite, we have that $\text{Var}(c_j(a_j, \xi_j) + r(a_j, \psi_\omega)) < +\infty$. For notational convenience, we define:

$$\varsigma^2(a_j) = \text{Var}(c_j(a_j, \xi_j) + r(a_j, \psi_\omega)).$$

Due to the law of large numbers, $g^M(a_j)$ pointwise converges to $g(a_j)$ w.p.1. By Chebyshev's inequality, for every fixed $a_j \in A_j$ and every $\varepsilon > 0$ there exists an $M(a_j, \varepsilon) \in \mathbb{Z}^+$ such that for all $m > M(a_j, \varepsilon)$ we have that:

$$\text{Prob}\{|g^m(a_j) - g(a_j)| < \varepsilon\} \geq 1 - \frac{\varsigma^2(a_j)}{m\varepsilon}.$$

Define:

$$\varsigma^2_{\max} = \sup_{a_j \in A_j} \varsigma^2(a_j);$$

and:

$$M(\varepsilon) = \max_{a_j \in A_j} M(a_j, \varepsilon);$$

for any $\varepsilon > 0$. Thus, for all $a_j \in A_j$ and for all $\varepsilon > 0$, we have that:

$$\text{Prob}\left\{|g^m(a_j) - g(a_j)| < \varepsilon\right\} \geq 1 - \frac{\varsigma_{\max}^2}{m\varepsilon};$$

if $m > M(\varepsilon)$. Therefore, $g^M(a_j)$ converges to $g(a_j)$ uniformly on $A_j$ w.p.1 as $M \to +\infty$. □

## Appendix E. Proof of Proposition 4

*Proof.* To show that $r(a_j, \psi_\omega)$ is Lipschitz continuous, we need to show that there exists a Lipschitz constant, $\mathcal{N}(\psi)$, such that:

$$|r(a_j^1, \psi_\omega) - r(a_j^2, \psi_\omega)| \leq \mathcal{N}(\psi)\|a_j^1 - a_j^2\|;$$

w.p.1 for all $a_j^1, a_j^2 \in A_j$.

From Proposition 2 we know that $r(a_j, \psi_\omega)$ is finite for almost every $\psi_\omega \in \Psi$. We further know that $r(a_j, \psi_\omega)$ is piecewise-linear convex on $A_j$. Thus, $r(a_j, \psi_\omega)$ is subdifferentiable and has finite subgradients for all $a_j \in A_j$ and almost every $\psi_\omega \in \Psi$. Thus, there must exist a finite Lipschitz constant, $\mathcal{N}(\psi)$, such that the Lipschitz condition is satisfied for almost every $\psi_\omega \in \Psi$. This implies that the Lipschitz constant has a finite MGF. Therefore, $r(a_j, \psi_\omega)$ is Lipschitz continuous w.p.1. □

## References


Bayraksan, G., Morton, D. P., September 2006. Assessing solution quality in stochastic programs. Mathematical Programming 108, 495–514.

Bayraksan, G., Morton, D. P., July-August 2011. A Sequential Sampling Procedure for Stochastic Programming. Operations Research 59, 898–913.

Bayram, İ. Ş., Michailidis, G., Papapanagiotou, I., Devetsikiotis, M., 9-13 December 2013. Decentralized control of electric vehicles in a network of fast charging stations. In: 2013 IEEE Global Communications Conference (GLOBECOM). Institute of Electrical and Electronics Engineers, Atlanta, GA, pp. 2785–2790.

Clement-Nyns, K., Haesen, E., Driesen, J., February 2010. The Impact of Charging Plug-In Hybrid Electric Vehicles on a Residential Distribution Grid. IEEE Transactions on Power Systems 25, 371–380.

Dobos, A. P., September 2014. PVWatts Version 5 Manual. Tech. Rep. NREL/TP-6A20-62641, National Renewable Energy Laboratory.

Gong, Q., Midlam-Mohler, S., Marano, V., Rizzoni, G., 25-26 May 2011. PEV Charging Impact on Residential Distribution Transformer Life. In: 2011 IEEE Energytech. Institute of Electrical and Electronics Engineers, Cleveland, OH, United States.

He, F., Wu, D., Yin, Y., Guan, Y., January 2013. Optimal deployment of public charging stations for plug-in hybrid electric vehicles. Transportation Research Part B: Methodological 47, 87–101.

He, F., Yin, Y., Wang, J., Yang, Y., March 2016. Optimal Prices of Electricity at Public Charging Stations for Plug-in Electric Vehicles. Networks and Spatial Economics 16, 131–154.

Hu, J., You, S., Lind, M., Østergaard, J., March 2014. Coordinated Charging of Electric Vehicles for Congestion Prevention in the Distribution Grid. IEEE Transactions on Smart Grid 5, 703–711.

Kariuki, K. K., Allan, R. N., March 1996. Evaluation of reliability worth and value of lost load. IEE Proceedings—Generation, Transmission, and Distribution 143, 171–180.

Kuby, M. J., Kelley, S. B., Schoenemann, J., December 2013. Spatial refueling patterns of alternative-fuel and gasoline vehicle drivers in Los Angeles. Transportation Research Part D: Transport and Environment 25, 84–92.

Ma, Z., Callaway, D. S., Hiskens, I. A., January 2013. Decentralized Charging Control of Large Populations of Plug-in Electric Vehicles. IEEE Transactions on Control Systems Technology 21, 67–78.

Momber, I., Siddiqui, A., Gómez San Román, T., Söder, L., March 2015. Risk Averse Scheduling by a PEV Aggregator Under Uncertainty. IEEE Transactions on Power Systems 30, 882–891.

Pantoš, M., May 2012. Exploitation of Electric-Drive Vehicles in Electricity Markets. IEEE Transactions on Power Systems 27, 682–694.

Razeghi, G., Zhang, L., Brown, T., Samuelsen, S., 15 April 2014. Impacts of plug-in hybrid electric vehicles on a residential transformer using stochastic and empirical analysis. Journal of Power Sources 252, 277–285.

Rotering, N., Ilić, M., August 2011. Optimal Charge Control of Plug-In Hybrid Electric Vehicles in Deregulated Electricity Markets. IEEE Transactions on Power Systems 26, 1021–1029.

Sathaye, N., September 2014. The optimal design and cost implications of electric vehicle taxi systems. Transportation Research Part B: Methodological 67, 264–283.

Sener, I. N., Ferdous, N., Bhat, C. R., Reeder, P., October 2009. Tour-Based Model Development for TxDOT: Evaluation and Transition Steps. Tech. Rep. FHWA/TX-10/0-6210-2, Center for Transportation Research at The University of Texas at Austin, Austin, Texas.

Sengupta, M., Habte, A., Gotseff, P., Weekley, A., Lopez, A., Anderberg, M., Molling, C., Heidinger, A., September 2014a. A Physics-Based GOES Product for Use in NREL's National Solar Radiation Database. Tech. Rep. NREL/CP-5D00-62776, National Renewable Energy Laboratory.

Sengupta, M., Habte, A., Gotseff, P., Weekley, A., Lopez, A., Molling, C., Heidinger, A., July 2014b. A Physics-Based GOES Satellite Product for Use in NREL's National Solar Radiation Database. Tech. Rep. NREL/CP-5D00-62237, National Renewable Energy Laboratory.

Shapiro, A., Dentcheva, D., Ruszczyński, A., 2014. Lectures on Stochastic Programming: Modeling and Theory, 2nd Edition. Society for Industrial and Applied Mathematics, Philadelphia, Pennsylvania.

Sundström, O., Binding, C., March 2012. Flexible Charging Optimization for Electric Vehicles Considering Distribution Grid Constraints. IEEE Transactions on Smart Grid 3, 26–37.

Wang, J., Liu, C., Ton, D., Zhou, Y., Kim, J., Vyas, A., July 2011. Impact of plug-in hybrid electric vehicles on power systems with demand response and wind power. Energy Policy 39, 4016–4021.

Weiller, C., June 2011. Plug-in hybrid electric vehicle impacts on hourly electricity demand in the United States. Energy Policy 39, 3766–3778.

Wu, C., Mohsenian-Rad, H., Huang, J., March 2012. Vehicle-to-Aggregator Interaction Game. IEEE Transactions on Smart Grid 3, 434–442.

Wu, F., Sioshansi, R., June 2017. A Stochastic Flow-Capturing Model to Optimize the Location of Fast-Charging Stations with Uncertain Electric Vehicle Flows. Transportation Research Part D: Transport and Environment 53, 354–376.

Xi, X., Sioshansi, R., May 2014. Using Price-Based Signals to Control Plug-in Electric Vehicle Fleet Charging. IEEE Transactions on Smart Grid 5, 1451–1464.

Xi, X., Sioshansi, R., January 2016. A Dynamic Programming Model of Energy Storage and Transformer Deployments to Relieve Distribution Constraints. Computational Management Science 13, 119–146.